

SANDIA REPORT

SAND2005-7941

Unlimited Release

Printed December 2005

Structure and Dynamics of Microbe-Exuded Polymers and Their Interactions with Calcite Surfaces

Thomas D. Perry, Randall T. Cygan, and Ralph Mitchell

Prepared by
Sandia National Laboratories
Albuquerque, New Mexico 87185 and Livermore, California 94550

Sandia is a multiprogram laboratory operated by Sandia Corporation, a Lockheed Martin Company, for the United States Department of Energy's National Nuclear Security Administration under Contract DE-AC04-94AL85000.

Approved for public release; further dissemination unlimited.



Issued by Sandia National Laboratories, operated for the United States Department of Energy by Sandia Corporation.

NOTICE: This report was prepared as an account of work sponsored by an agency of the United States Government. Neither the United States Government, nor any agency thereof, nor any of their employees, nor any of their contractors, subcontractors, or their employees, make any warranty, express or implied, or assume any legal liability or responsibility for the accuracy, completeness, or usefulness of any information, apparatus, product, or process disclosed, or represent that its use would not infringe privately owned rights. Reference herein to any specific commercial product, process, or service by trade name, trademark, manufacturer, or otherwise, does not necessarily constitute or imply its endorsement, recommendation, or favoring by the United States Government, any agency thereof, or any of their contractors or subcontractors. The views and opinions expressed herein do not necessarily state or reflect those of the United States Government, any agency thereof, or any of their contractors.

Printed in the United States of America. This report has been reproduced directly from the best available copy.

Available to DOE and DOE contractors from

U.S. Department of Energy
Office of Scientific and Technical Information
P.O. Box 62
Oak Ridge, TN 37831

Telephone: (865)576-8401
Facsimile: (865)576-5728
E-Mail: reports@adonis.osti.gov
Online ordering: <http://www.doe.gov/bridge>

Available to the public from

U.S. Department of Commerce
National Technical Information Service
5285 Port Royal Rd
Springfield, VA 22161

Telephone: (800)553-6847
Facsimile: (703)605-6900
E-Mail: orders@ntis.fedworld.gov
Online order: <http://www.ntis.gov/help/ordermethods.asp?loc=7-4-0#online>



SAND2005-7941
Unlimited Release
Printed December 2005

Structure and Dynamics of Microbe-Exuded Polymers and Their Interactions with Calcite Surfaces

Thomas D. Perry
Division of Engineering and Applied Sciences
Harvard University
Cambridge, Massachusetts 02138

Randall T. Cygan
Geochemistry Department
Sandia National Laboratories
Albuquerque, New Mexico 87185-0754

Ralph Mitchell
Division of Engineering and Applied Sciences
Harvard University
Cambridge, Massachusetts 02138

Abstract

Cation binding by polysaccharides is observed in many environments and is important for predictive environmental modeling, and numerous industrial and food technology applications. The complexities of these organo-cation interactions are well suited to predictive molecular modeling studies for investigating the roles of conformation and configuration of polysaccharides on cation binding. In this study, alginic acid was chosen as a model polymer and representative disaccharide and polysaccharide subunits were modeled. The ability of disaccharide subunits to bind calcium and to associate with the surface of calcite was investigated. The findings were extended to modeling polymer interactions with calcium ions.

Acknowledgements

This work was supported by Sandia's Laboratory Directed Research and Development (LDRD) Project 69158. Todd Perry is the recipient of a Sandia National Laboratories Campus Executive Fellowship sponsored by the LDRD program. Ralph Mitchell is grateful for support received from the U. S. National Science Foundation and W. R. Grace Corporation. Randall Cygan acknowledges the support provided by the Chemical Sciences, Geosciences, and Biosciences Division of the Office of Basic Energy Sciences in the U.S. Department of Energy. Sandia is a multiprogram laboratory operated by Sandia Corporation, a Lockheed Martin Company, for the United States Department of Energy's National Nuclear Security Administration under Contract DE-AC04-94AL85000.

Table of Contents

1. Introduction	7
2. Approach	11
2.1. Polymer structure.....	11
2.2. Theoretical Approach	11
2.2.1. Study of Alginic Acid Configuration Using CVFF.....	11
2.2.2. Study of Alginic Acid in the Presence of Calcite Using a New Hybrid Force Field.....	11
2.3. Computational Methods	15
2.3.1. Conformational Analysis of Disaccharides and Polysaccharides	15
2.3.2. Molecular Dynamics Simulations of Disaccharides and Polysaccharides Cluster Models.....	16
2.3.3. Simulation of Disaccharides in the Presence of a <u>(10$\bar{1}$4)</u> Calcite Surface	17
3. Results and Discussion	19
3.1. Torsional Conformation of Disaccharides.....	19
3.2. Molecular Dynamics Simulations with Disaccharides.....	25
3.3. Molecular Dynamics Simulations with Polymers	28
3.4. Association of Calcium Ions with Disaccharides and Polymers	28
3.5. Simulations with Alginic Acid Disaccharides and the <u>(10$\bar{1}$4)</u> Calcite Face.....	32
3.6. Alginic Acid Binding at a Surface Defect on the Calcite Surface.....	41
4. Conclusions	43
5. References	45

Figures

1	Chemical structure of alginic acid	11
2	Examples of periodic simulation cells of solvated and surface-sorbed systems	18
3	Molecular dynamics simulation of torsional changes of mannuronic disaccharides.....	21
4	Molecular dynamics simulation of torsional changes of guluronic disaccharides	22
5	Molecular dynamics simulation of torsional changes of mannuronic-guluronic dimer	23
6	Molecular dynamics simulation of disaccharides started at local minimum at 300 K	26
7	Molecular dynamics simulation of disaccharides started at local minima at 400 K.....	26
8	Molecular dynamics simulation of polysaccharides consisting of twenty units at 300 K....	29
9	Molecular dynamics simulation of polysaccharides consisting of twenty units at 400 K....	30
10	Energy-minimized structures of alginic acid associated with calcium ions	31
11	Energy-minimized structures of polymers in different torsional conformations.....	33
12	Average potential energy of the simulations cells and disaccharide sorption energy	35
13	Results of molecular dynamics simulations of the <i>GG</i> on calcite surface.....	37

14	Radial distribution functions for Ca-O interactions from <i>GG</i> -calcite simulation.....	38
15	Variation in torsion angles and potential energy of the solvated <i>GGb</i> disaccharide	38
16	Surface structures from the molecular dynamics simulation of the <i>GG</i> disaccharide	40
17	View of the energy-minimized conformations of <i>GG-a</i> disaccharides on calcite pit.....	42

Tables

1	Atom types and descriptions	12
2	Expressions for hybrid force field functionality	13
3	Force field parameters for the carbonate-water-organic interactions	14
4	Potential energy minima of torsional conformations of alginic acid disaccharides	20
5	Torsional variation of protonated and deprotonated alginic acid disaccharides.....	27
6	Proximity of oxygen moieties to calcium during chelation by deprotonated alginic acid....	32
7	Torsional variation of the ether linkage during molecular dynamic simulations	34

1. Introduction

Modeling and prediction of cation binding as determined by polysaccharide structure is desirable for a variety of industrial applications that require the dissolution of metal-bearing minerals (Jamialahmadi and Mullersteinhagen, 1991; Moore et al., 1972), and is important for understanding cation binding in the environment and geochemical speciation-transport modeling. Calcite (calcium carbonate) mineralization (dissolution and precipitation) is important in biological, environmental, and industrial systems. In the environment, calcite is an important reservoir of carbon, and accelerated dissolution of calcite affects global carbon cycling (Schlesinger, 1997), the chemistry of marine systems (Pilson, 1998), and the local pH and alkalinity of terrestrial environments (Stumm and Morgan, 1996). Calcite and other carbonate phases are the primary pH buffer in many natural waters, and calcite weathering impacts porosity and heterogeneity in aquifers, which, in turn, leads to hydrologic complexity in reactive transport modeling (Stumm, 1992). In terrestrial environments calcite dissolution partially regulates the fate and transport of anthropogenic pollutants, especially heavy metals (Reeder et al., 2001). In industrial systems, calcite scale develops on water pipes and can reduce heat-transfer efficiency dramatically (Stahl et al., 2000).

Interaction of organic species with the calcite surface has been observed to control dissolution rates. Synthetically-derived chelating agents, including polyaspartic acid (PASP), ethylenediamine tetraacetic acid (EDTA), diethylenetriaminepentaacetic acid (DTPA), and 1,2-cyclohexanediaminetetraacetic acid (CTDA) increase the dissolution rate of calcite (Fredd and Fogler, 1998; Perry et al., 2005; Wu and Grant, 2002) and are employed to assist in the dissolution of calcium-bearing minerals for industrial applications, such as the renewal of petroleum wells clogged by calcite (Fredd and Fogler, 1998) and the removal of scale from boilers and heater tubes (Jamialahmadi and Mullersteinhagen, 1991; Moore et al., 1972). Biogenic ligands (Orme et al., 2001; Teng et al., 1998) are also important in regulating calcite dissolution in marine and terrestrial systems (Pilson, 1998; Stumm and Morgan, 1996). Many biologically-derived compounds, however, inhibit dissolution, including lipids and phospholipids (Suess, 1970), proteins (Suess, 1970), humics (Hoch et al., 2000), and other carboxylated compounds (Fredd and Fogler, 1998), though the effect varies widely with chemical identity and aqueous conditions (Compton and Sanders, 1993; Thomas et al., 1993). Some biologically-derived compounds have been observed to interact specifically with different calcite faces during dissolution (Perry et al., 2004) and precipitation (Orme et al., 2001). Polysaccharides have been observed to bind to cations on mineral surfaces, both inhibiting and promoting dissolution (Thomas et al., 1993; Welch and Vandevivere, 1994). The distinctive dissolution effects of organic ligands depend strongly on their chemistry but an atomistic understanding of these organic-mineral interactions remains elusive.

Interaction of organic macromolecules with calcite can also result in controlled precipitation in some biological systems. Organisms, including algae (coccoliths) (Henriksen et al., 2003), sea urchins (Berman et al., 1988), brittlestars (Aizenberg et al., 2001), trilobites (Fortey and Chatterton, 2003), and higher organisms (Söllner et al., 2003) manipulate calcite crystal structure, kinetics, and localization during precipitation for the controlled growth of optic structures (Teng et al., 1998). Crystal shape is controlled by step-specific interactions between growth modifiers and individual step edges on preexisting crystal faces (De Yoreo and Dove,

2004; Orme et al., 2001). The interactions of organic additives with particular microscopic steps on crystal faces during growth result in altered macroscopic morphologies unexpressed in pure systems (Teng et al., 1998). Changes in the elementary growth step generate a similarly modified bulk crystal shape through the self-replicating process of crystal growth. The emergence of new crystal faces is therefore a macroscopic manifestation of the kinetics caused by molecular-scale interactions at the step edges (De Yoreo and Dove, 2004). Similarly, these interactions remain poorly understood, in part, due to the difficulty modeling them at the atomic scale.

In continental environments, polysaccharides are the second most abundant organic species following humic substances and can range from 5 to 30% in concentration of the total organic matter (Martin, 1971). Many of these compounds are extracellular polysaccharides (EPS) produced in microbial biofilms—thin films of microorganisms, including bacteria, Archaea, cyanobacteria, algae, fungi, and lichens, growing on surfaces in an excreted layer of polysaccharide (Christensen and Charaklis, 1990; Saiz-Jimenez, 1999). The composition of EPS produced by microorganisms is genotypically, phenotypically, and environmentally regulated. Polysaccharides are the dominant constituent of biofilms, which are semi-rigid materials due to cation bridging that cross-link and “gel” the polymers. The polysaccharides are generally comprised of a variety of sugars and often contain functional groups (such as carboxylic acids) that can interact with cations. The specific cation binding effects of polysaccharides depend on polysaccharide conformation and configuration, ligand functionality, acidic moieties, length of the uncomplexed blocks between the cross-linked regions, cation type, and pH (Sabra et al., 2001).

Alginic acid was selected as a model environmental polysaccharide due to its demonstrated presence in the environment and well-characterized chemistry. It is a straight-chain, hydrophilic, colloidal, polyuronic acid typically arranged in three combinations of disaccharide subunits: α -L-(1-4) guluronic-guluronic (*GG*), α -L-(1-4) mannuronic-guluronic (*MG*), β -D-(1-4) mannuronic-mannuronic (*MM*). Henceforth, the subunits will be referred to as *GG*, *MG*, and *MM*. The guluronic-mannuronic disaccharide also exists but was excluded from the present study for brevity. Approximately 20-50% of polysaccharides produced in a wide sampling of marine and terrestrial bacteria were uronic acids (Kennedy and Sutherland, 1987). Alginic acid is a dominant environmental polymer produced by seaweed in marine environments (Davis et al., 2003), and by environmental bacteria including *Azotobacter vinelandii* and *Pseudomonas aeruginosa* (Boyd and Chakrabarty, 1995), which is a ubiquitous environmental bacterium (Hardalo and Edberg, 1997; Wolfgang et al., 2003). There are structural differences between alginates produced by algae and bacteria, including the relative ratios and arrangements of the different monosaccharide blocks and acetylation at the C-2 and C-3 positions of the bacterial alginate (Lattner et al., 2003).

Empirical studies have demonstrated that the electron donating moieties of alginic acid polymers are responsible for chelating aqueous cations such as Ca^{2+} (Davis et al., 2003). Alginic acid specifically interacts with crystallographic features of calcite (Didymus et al., 1993; Perry et al., 2004) and can increase the dissolution rate of calcite (Perry et al., 2004) and other minerals (Welch et al., 1999). The electron-donating moieties of alginic acid, including all of the negatively-charged oxygen atoms in the disaccharides, namely, hydroxyl oxygens, ether

oxygens, and carboxylate oxygens, chelate aqueous cations (Figure 1 of Davis et al., 2003) at intermediate to high pH conditions. The carboxyl functional groups of *GG*-blocks have appropriate spacing and geometry for cation binding (Dheu-Andries and Pérez, 1983), and *GG*-blocks have a higher affinity for divalent cation binding than their *MM* counterparts (Smidsrød and Haug, 1965). As a result, the proportion of *MM*- and *GG*-blocks and their macromolecular conformation determine the physical properties and the affinity of the polymer for cation binding (Haug et al., 1967). Cation binding can be ordered or disordered (Braccini and Pérez, 2001) as determined by the proportion of *GG*- and *MM*-blocks and their macromolecular conformation (Haug et al., 1967). The carboxylate functional groups of *GG*-blocks have appropriate spacing and geometry for cation binding in solution, especially for calcium ions (Dheu-Andries and Pérez, 1983), imparting *GG*-blocks with a higher affinity for divalent cation binding than *MM*-blocks (Smidsrød and Haug, 1965). Planar *MM*-blocks also bind calcium ions, although the association is less ordered than for *GG* because they do not have the correct special and geometric arrangement for binding sites (Grant et al., 1973).

Cation binding and gelling of alginic acid are important aspects of this macromolecule. A detailed molecular level understanding of the complex chemical contributions to cation binding is essential to understand fully this phenomenon. The use of molecular modeling methods such as energy optimization and molecular dynamics in this study allows access to additional insights that may be difficult, if not impossible, to obtain experimentally (Guimarães et al., 2004) and ultimately broadens the understanding of these chemical interactions. Also, a fundamental understanding of the atomistic interactions of organic species with mineral surfaces during dissolution and precipitation needs to be developed (Banfield et al., 1999; Welch and Vandevivere, 1994). Predictive molecular simulation requires development of empirical energy force fields that can accurately simulate inter- and intra-molecular interactions in complex, heterogeneous systems with different and numerous molecular types (Kollman, 1996). Previous modeling efforts have been limited by the availability of an energy force field that can simultaneously simulate these complicated systems. Attempts to model different aspects of the systems have been performed using static calculations (de Leeuw and Cooper, 2004), in vacuo (Duckworth et al., 2003), by focusing on the interaction of organics with cations (Braccini et al., 1999) and water (Guimarães et al., 2004), by modeling minerals with monolayers of water (Kerisit and Parker, 2004), or by combination of potential models (de Leeuw and Cooper, 2004). To our knowledge, no previous study has developed a general and accurate set of force field parameters to model the interactions of organic species, with water, calcium ions, and the carbonate substrate.

This study presents a comprehensive approach for determination of disaccharide and polysaccharide structure as determined by monosaccharide configuration and conformation. The structural stability is tested in the presence of calcium cations and at elevated temperature. Using a newly developed force field, the structures and energetics of these organic materials are evaluated with and without a calcite surface. The approach and results will be of interest to computational and environmental chemists and geochemists. A modified version of the report has been submitted to the journal *Geochimica et Cosmochimica Acta* and is expected to be published in early 2006.

2. Approach

2.1. Polymer Structure

Schematic representations of the three primary polymeric subunits of alginic acid used in the molecular simulations are shown in Figure 1. These structures are empirically confirmed in several independent analyses of natural alginic acid (Evans and Linker, 1973). The conformations of disaccharides are largely defined by two torsion angles linking the sugar rings: $\Phi = O^{5'} \rightarrow C^{1'} \rightarrow O^4 \rightarrow C^4$ and $\Psi = C^{1'} \rightarrow O^4 \rightarrow C^4 \rightarrow C^5$ (Figure 1) (Braccini et al., 1999).

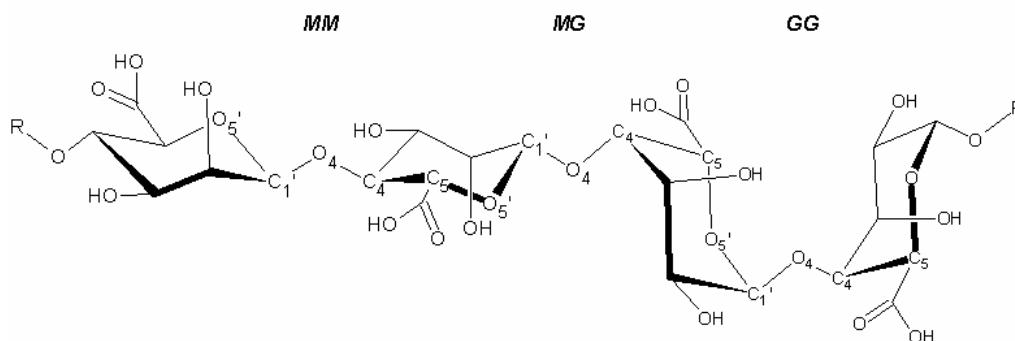


Figure 1. Chemical structure of alginic acid.

2.2. Theoretical Approach

2.2.1. Study of Alginic Acid Configuration Using CVFF

The Consistent Valence Force Field (CVFF) was originally designed for investigating peptide and protein structures (Dauber-Osguthorpe et al., 1988) but recently has been successfully applied to polysaccharides (Hoog et al., 2002) and to organic macromolecule-calcium ion interactions (Iyer and Qasba, 1999). CVFF describes the energy of a chemical system through summation of individual interatomic energies and the geometry of the molecular configuration (Cygan, 2001). The energy values reported in this study are based on the potential models within CVFF and can be used to interpret relative conformational stability but are not necessarily absolute quantities. The bonded terms usually dominate the structure determination of neutral organic molecules, while the nonbonded terms become increasingly important in charged or polar systems, including the simulation of calcium ion-alginate disaccharides and polymer systems. This force field was used to analyze alginic acid structure in the absence and presence of free calcium cations.

2.2.2. Study of Alginic Acid in the Presence of Calcite Using a New Hybrid Force Field

The CVFF force field was not designed for simulating crystalline materials such as the bulk and surface structures of calcite. Hence, a new force field was developed with optimized interatomic potentials for organic molecule interaction with a carbonate mineral surface with explicit water molecules to represent a hydrated environment. We had successfully developed an energy force

field capable of simulating a carbonate mineral surface with partial and full water hydration (Perry et al., 2006). Further development of the force field for the present study allowed inclusion of interaction parameters for the organic components of the alginic acid units. Atom typing and descriptions (Table 1), expressions for hybrid force field functionality (Table 2), and parameters for the carbonate-water-organic interactions (Table 3) are summarized. Parameters for the organic components are taken from the CVFF force field (Dauber-Osguthorpe et al., 1988). Van der Waals interactions presented in Table 3 were derived through the use combination rules (Halgren, 1992) and the conversion of Buckingham style potentials (Duckworth et al., 2003) to the standard Lennard-Jones potential (see Table 2).

Table 1. Atom types and descriptions.

Element	Description	Symbol	Charge (e)
H	water hydrogen	<i>h*</i>	0.4100
O	water oxygen	<i>o*</i>	-0.8200
O	carbonate oxygen	<i>o</i>	-1.1145
C	carbonate carbon	<i>c</i>	1.3435
Ca	calcium	<i>Ca</i>	2.0000
H	alkane hydrogen	<i>h</i>	0.1000
H	hydroxyl hydrogen	<i>ho</i>	0.3500
C	alkane carbon	<i>cI</i>	-0.0700
C	carboxyl carbon	<i>c'</i>	0.4100
C	carboxylate carbon	<i>c-</i>	0.1400
O	ether oxygen	<i>oe</i>	-0.3000
O	carboxyl oxygen	<i>o'</i>	-0.3800
O	carboxylate oxygen	<i>o-</i>	-0.5700
O	hydroxyl oxygen	<i>oh</i>	-0.3800

Table 2. Expressions for hybrid force field functionality.

Total Energy
$E_{total} = E_{Coul} + E_{VDW} + E_{bondstretch} + E_{anglebend} + E_{inversions} + E_{torsions}$
Coulombic energy (E_{Coul})
$E_{Coul} = \frac{e^2}{4\pi\epsilon_o} \sum_{i \neq j} \frac{q_i q_j}{r_{ij}}$
van der Waals energy (E_{VDW})
$E_{VDW} = \sum_{i \neq j} D_{o,ij} \left[\left(\frac{R_{o,ij}}{r_{ij}} \right)^{12} - 2 \left(\frac{R_{o,ij}}{r_{ij}} \right)^6 \right]$
Bond stretch energy ($E_{bondstretch}$) of the hydroxyl
$E_{bondstretch,ij}^{o^*-h^*} = \frac{1}{2} k_1 (r_{ij} - r_o)^2$
Bond stretch energy ($E_{bondstretch}$) of the carbonate
$E_{bondstretch,ij}^{c-o} = D_e (e^{-\alpha(r-r_o)} - 1)^2$
Angle bend energy ($E_{anglebend}$)
$E_{anglebend,ijk} = \frac{1}{2} k_2 (\theta_{ijk} - \theta_o)^2$
Bond inversion energy ($E_{inversion}$) of the carbonate
$E_{inversion,ijkl} = \frac{1}{2} k_i (1 + \cos \phi)^2$
Torsion energy ($E_{torsion}$) of the organics
$E_{torsion,ijkl} = \sum_j \left\{ \left(\frac{1}{2} k_t \right) (1 - n \cos \phi) \right\}$

Table 3. Force field parameters for the carbonate-water-organic interactions.

Interacting atoms			
species <i>i</i>	species <i>j</i>	R_o (Å)	D_o (kcal/mol)
<i>o</i> *	<i>o</i> *	3.5532	1.5540E-01
<i>o</i>	<i>o</i> *	4.4266	6.9687E-05
<i>o</i>	<i>o</i>	5.9000	4.5000E-08
<i>Ca</i>	<i>o</i> *	5.6000	3.4000E-04
<i>Ca</i>	<i>o</i>	4.9460	1.4555E-03
<i>h</i>	<i>o</i> *	3.1516	7.6845E-02
<i>h</i>	<i>o</i>	4.0250	3.4460E-05
<i>h</i> *	<i>o</i>	4.0250	3.4460E-05
<i>ho</i>	<i>o</i>	4.0250	3.4460E-05
<i>h</i>	<i>Ca</i>	3.6710	1.6051E+00
<i>c</i>	<i>o</i> *	3.8066	1.5165E-01
<i>cI</i>	<i>o</i> *	3.9516	7.7850E-02
<i>cI</i>	<i>o</i>	4.8250	3.4911E-05
<i>cI</i>	<i>Ca</i>	4.4710	1.6261E+00
<i>cI</i>	<i>h</i>	3.4587	3.8497E-02
<i>cI</i>	<i>cI</i>	4.3500	3.9000E-02
<i>c'</i>	<i>o</i> *	3.8066	1.5165E-01
<i>c'</i>	<i>o</i>	4.6800	6.8007E-05
<i>c'</i>	<i>Ca</i>	4.3260	3.1676E+00
<i>c'</i>	<i>h</i>	3.3414	7.4993E-02
<i>c'</i>	<i>cI</i>	4.2025	7.5974E-02
<i>c'</i>	<i>c'</i>	4.0600	1.4800E-01
<i>c-</i>	<i>o</i> *	3.8066	1.5165E-01
<i>c-</i>	<i>o</i>	4.6800	6.8007E-05
<i>c-</i>	<i>Ca</i>	4.3260	3.1676E+00
<i>c-</i>	<i>h</i>	3.3414	7.4993E-02
<i>c-</i>	<i>cI</i>	4.2025	7.5974E-02
<i>c-</i>	<i>c'</i>	4.0600	1.4800E-01
<i>c-</i>	<i>c-</i>	4.0600	1.4800E-01
<i>oe</i>	<i>o</i> *	3.3816	1.8823E-01
<i>oe</i>	<i>o</i>	4.2550	8.4410E-05
<i>oe</i>	<i>Ca</i>	3.9010	3.9316E+00
<i>oe</i>	<i>h</i>	2.9711	9.3081E-02
<i>oe</i>	<i>cI</i>	3.7368	9.4297E-02
<i>oe</i>	<i>c'</i>	3.6101	1.8370E-01
<i>oe</i>	<i>c-</i>	3.6101	1.8370E-01
<i>oe</i>	<i>oe</i>	3.2100	2.2800E-01
<i>o'</i>	<i>o</i> *	3.3816	1.8823E-01
<i>o'</i>	<i>o</i>	4.2550	8.4410E-05
<i>o'</i>	<i>Ca</i>	3.9010	3.9316E+00
<i>o'</i>	<i>h</i>	2.9711	9.3081E-02
<i>o'</i>	<i>cI</i>	3.7368	9.4297E-02
<i>o'</i>	<i>c'</i>	3.6101	1.8370E-01

Table 3. continued

<i>o'</i>	<i>c-</i>	3.6101	1.8370E-01
<i>o'</i>	<i>oe</i>	3.2100	2.2800E-01
<i>o'</i>	<i>o'</i>	3.2100	2.2800E-01
<i>o-</i>	<i>o*</i>	3.3816	1.8823E-01
<i>o-</i>	<i>o</i>	4.2550	8.4410E-05
<i>o-</i>	<i>Ca</i>	3.9010	3.9316E+00
<i>o-</i>	<i>h</i>	2.9711	9.3081E-02
<i>o-</i>	<i>cI</i>	3.7368	9.4297E-02
<i>o-</i>	<i>c'</i>	3.6101	1.8370E-01
<i>o-</i>	<i>c-</i>	3.6101	1.8370E-01
<i>o-</i>	<i>oe</i>	3.2100	2.2800E-01
<i>o-</i>	<i>o'</i>	3.2100	2.2800E-01
<i>o-</i>	<i>o-</i>	3.2100	2.2800E-01
<i>oh</i>	<i>o*</i>	3.3816	1.8823E-01
<i>oh</i>	<i>o</i>	4.2550	8.4410E-05
<i>oh</i>	<i>Ca</i>	3.9010	3.9316E+00
<i>oh</i>	<i>h</i>	2.9711	9.3081E-02
<i>oh</i>	<i>cI</i>	3.7368	9.4297E-02
<i>oh</i>	<i>c'</i>	3.6101	1.8370E-01
<i>oh</i>	<i>c-</i>	3.6101	1.8370E-01
<i>oh</i>	<i>oe</i>	3.2100	2.2800E-01
<i>oh</i>	<i>o'</i>	3.2100	2.2800E-01
<i>oh</i>	<i>o-</i>	3.2100	2.2800E-01
<i>oh</i>	<i>oh</i>	3.2100	2.2800E-01

2.3. Computational Methods

2.3.1. Conformational Analysis of Disaccharides and Polysaccharides

All molecular modeling simulations were performed using Cerius² software (Accelrys Inc., San Diego). Molecular geometries were obtained through energy minimization procedures based on an energy convergence value of 0.001 kcal mol⁻¹. Disaccharide conformations are determined primarily by the torsion of linkages between monomers and computer experiments investigated the local and global energy minima of the disaccharides as primarily determined by linkage torsions. The two principal torsion angles (Φ , Ψ) were rotated 360° simultaneously at 10° increments to allow an analysis of conformational energies. For each iteration, torsional bonds were spatially fixed, the remaining atoms of the disaccharide molecule were geometrically optimized, and the total energy was calculated for all atomic interactions. Excluding the linkage torsion of interest, this approach allows complete relaxation of the molecule including all other torsion angles, including those associated with hydroxyl and carboxylate functional groups. The relatively large increments of rotation were sufficient for detecting regions of potential energy minima. However, some artifacts of the incremental shifts were observed and were attributed to the inability of the bonds, especially those of stabilizing functional groups, to continuously minimize during incremental rotation. This artifact was ameliorated by using torsional values for minima from automated analysis as a starting point for a full geometry optimization. The full optimizations were initiated with the first-order conformation derived from the automated torsional analysis but allowed full atomic flexibility, thereby allowing all atoms and bonds to relax and energy minimize.

For Coulombic and van der Waals interactions in simulations with disaccharides, a spline cutoff distance of 8.5 Å was used; for polymers, a cutoff value of 55.0 Å was employed. The rationale for modifying the cutoff values for larger molecules is to assure that intramolecular interactions between atoms are included in calculations (Allen and Tildesley, 1987), which is especially important with large polymers that can exhibit significant intramolecular interactions (Sun et al., 1998). When there were significantly large energy instabilities or nonconvergence issues, those conformations were denoted by assigning an artificial energy value of +1000 kcal mol⁻¹. The previously successfully minimized conformation model was then reloaded and automatically advanced to the next simulation torsion angle increment to continue with the Φ - Ψ energy mapping. Reloading the previous model was important to lessen the effects of instability created by spatial rearrangements during the previous energy minimization, such as those involving the rearrangements of the torsions of the carboxylate. These potential energy map simulations were repeated with protonated and deprotonated (charge states of 0 and -2, respectively) *MM*, *GG*, and *MG* disaccharides and with dielectric constant (ϵ) values set at either 1 or 78. Calculations performed with $\epsilon = 1$ represent a vacuum environment where the Coulombic interactions are evaluated directly. Increasing the dielectric constant ($\epsilon = 78$) in the simulations effectively shields the intramolecular Coulombic interactions and mimics an aqueous environment where water molecules implicitly solvate the molecule (Guenot and Kollman, 1992). We acknowledge that at $\epsilon = 78$ the calculations are an approximation due to shielding of the 1-4 carbon interactions, which are of interest when modeling torsions (Braccini et al., 1999). However, this is not a critical concern because we are attempting to evaluate the conformation resulting in the lowest potential energy, i.e. the most stable conformation. At the dielectric values evaluated, the potential wells remain in the same position and are relatively unchanged, except in breadth and depth, which does not affect the region of determined stable conformation. Polymers were constructed from the resulting stable conformations of the disaccharides and molecular dynamic simulations were conducted, as described below.

For calculation of energy minima when the disaccharides bind with calcium ion, identified stable structures of deprotonated disaccharides as first determined above were manually docked with a cation and energetically minimized with $\epsilon = 1$. These simulations were performed on the isolated gas-phase model to identify first-order effects and determine if the binding of calcium can influence saccharide structure; detailed modeling should necessarily include explicit hydration, since the water molecules affect cation binding and competition with any aqueous phase. Relative stability of various configurations was assessed by manually interacting the calcium ion with different parts of the disaccharide. Additionally, short duration molecular dynamics simulations (less than 10 ps) were employed to evaluate relative stabilities. Following molecular dynamic simulations and conformation verification, polymers were constructed from calcium-associated disaccharides and these twenty-unit polysaccharides were subsequently energy minimized.

2.3.2. Molecular Dynamics Simulations of Disaccharides and Polysaccharides Cluster Models

Molecular dynamics calculations were performed on the various disaccharides and on constructed twenty-unit polysaccharides. All dynamics simulations were performed as canonical ensembles where volume and temperature conditions were maintained statistically constant (Allen and Tildesley, 1987). A Nosé-Hoover thermostat (Hoover, 1985) maintained at 300 K

was used to control temperature during the simulations, which were performed for periods of 100 ps with a relaxation time of 0.1 ps. The duration of these simulations is adequate to completely sample their conformational space; the molecules maintain the representative conformations associated with potential energy minima. The Verlet velocity algorithm was used to obtain accurate integration of the dynamics equations and statistical ensembles (Verlet, 1967). Polysaccharides were additionally subjected to an initial 20 ps equilibration run before the long-term simulation to ensure full equilibration of the system. A more detailed study of the interaction of the polysaccharides with calcium ions would necessarily include model simulations with more than a single polysaccharide chain; the present study, however, limited this effort to to emphasize the interactions of alginic acid with the calcite surface.

Molecular modeling of the structural conformations of the disaccharides identified global energy minimum (*a*) and local energy minimum (*b*) conformations, and those results are employed in the remainder of this study.

2.3.3. Simulation of Disaccharides in the Presence of a (10 $\bar{1}$ 4) Calcite Surface

The total dimensions of the simulation cell with periodic boundary conditions were 24.0 Å x 29.7 Å x 56.8 Å and consisted of an approximated 30 Å-deep solvation region above a 20 Å-deep substrate originally created from the (10 $\bar{1}$ 4) cleavage of calcite and the experimental crystal structure (Effenberger et al., 1981). All simulations contain the identical number of atoms and therefore potential energies, relative binding enthalpies, and identify stable configurations can be directly compared. Disaccharides are treated as dianionic species with the carboxylic groups deprotonated in order to represent the expected protonation state at neutral pH conditions (Belitz and Grosch, 1987). The dimensions of the simulation cell were important for minimizing interactions among periodic images of the reference cell. Periodic simulations were performed using spline cutoffs of 8 Å and 8.5 Å for the short-range van der Waals interactions and long-range Ewald sums for Coulombic interactions (Tosi, 1964). The molecular simulation methods were used for the periodic simulations. Due to the charged nature of the disaccharide anions, a compensating background charge is applied across the simulation cell to maintain neutrality. Simulations were allowed to equilibrate using a 1 fs time step for an initial 20 ps period followed by a 50 ps production period for obtaining equilibrium statistics on energy and structure. Results for the *MM-b* simulations are derived from the last stages of the 20 ps equilibration run due to transient instabilities in the 50 ps production run.

Disaccharides in solvated and surface-sorbed (surficial) systems were compared based on simulation results for sorption energies and ether-linkage torsions. Sorption energies (E_{sorp}) were calculated for each of the disaccharides according to the following:

$$E_{sorp} = E_{solv} - E_{surf} \quad (1)$$

where E_{solv} is the mean potential energy of the system when the disaccharide is solvated (far removed from the calcite-solution interface) and E_{surf} is the mean potential energy of the system when the disaccharide is located at the mineral surface with no intermediate water molecules (Figure 2) from the 50 ps simulations.

Results for molecular ordering and energetics at the calcite-water interface are presented in this study. Selected monolayers of calcite components (Ca^{2+} and CO_3^{2-}) and water were analyzed by quantifying the variation in density of constituent calcite atoms 3 Å into the calcite surface and water/disaccharide atoms 3.5 Å into the bulk solution. A complete data set is presented for the simulation of the *GG* disaccharide-calcite system. Similar simulations were conducted with the *MG* and *MM* disaccharides with calcite and are summarized and compared, but detailed presentation of the data has been omitted for brevity.

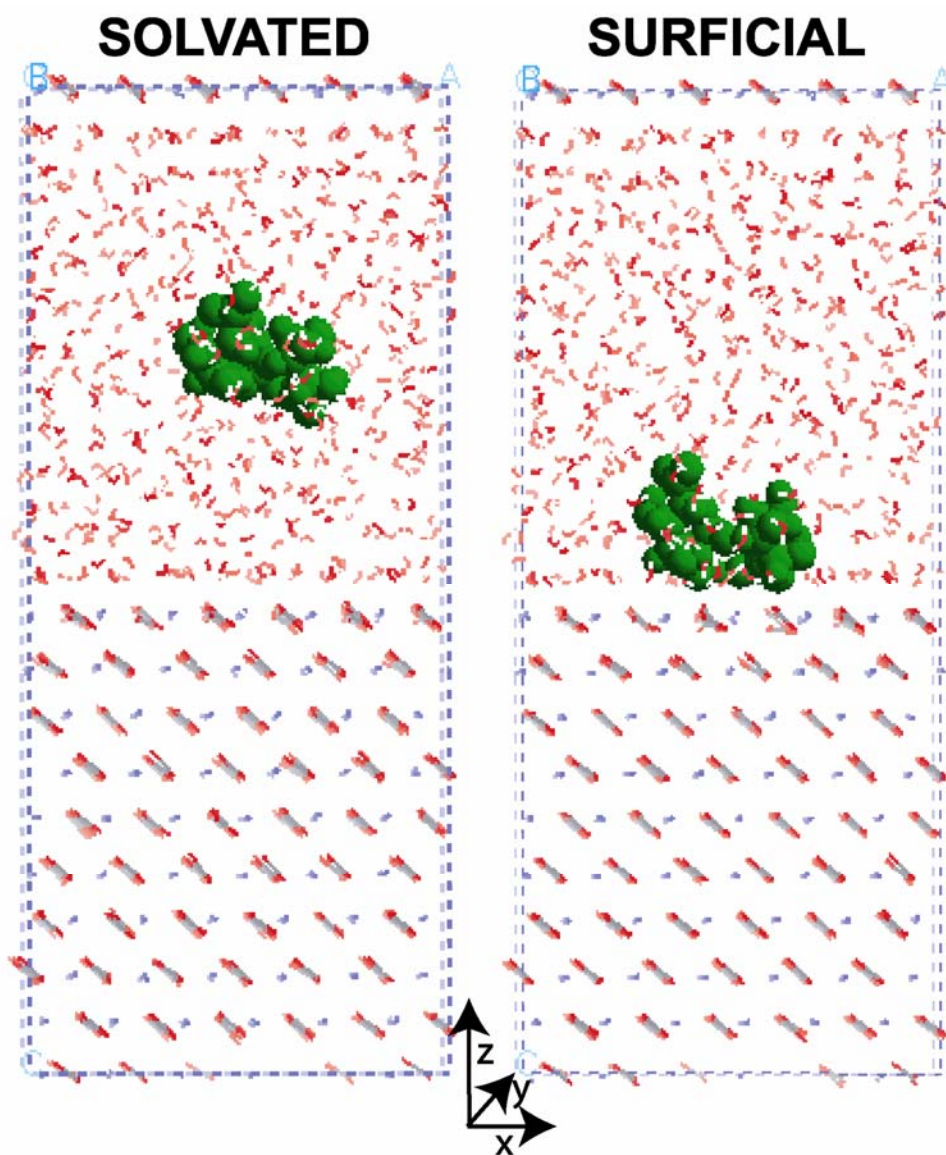


Figure 2. Examples of periodic simulation cells of solvated and surface-sorbed systems with the *GG-a* disaccharide and the $(10\bar{1}4)$ calcite face with explicit hydration. The disaccharides have been colored green to facilitate identification.

3. Results and Discussion

The following sections explore the energetics and torsion mechanics of alginic acid disaccharide subunits rotated about the ether linkage. Molecular dynamic simulations are mapped onto the potential energy surfaces to identify potential metastable conformations. Calcium binding of the geometry-optimized disaccharides was explored by the manual docking of calcium ion at binding sites of the various disaccharides. Minimized Ca^{2+} -disaccharide structures were then used to predict possible conformations of the Ca^{2+} -polymer complex. The determined structures of the alginic acid disaccharides were then interacted using explicit hydration at near (sorbed) and far (solvated) distances from a simulated $(10\bar{1}4)$ calcite surface and torsional behavior was observed during dynamic simulation. Finally, a disaccharide was interacted with a surface defect on the $(10\bar{1}4)$ calcite surface.

3.1. Torsional Conformation of Disaccharides

Alginic acid is produced in *MM*, *GG*, and alternating *MG* blocks. The different linkages between the monomers are the primary control on polymer structure, and torsion simulations were implemented to determine stable conformations of *MM*, *GG*, and *MG* disaccharides when protonated and deprotonated. The minimum (*a*) structure is defined as the global potential energy minimum for a particular disaccharide for the experimental conditions. Metastable local minima are assigned alphabetically (*b*, *c*, *d*) as energy increases (Table 4). In this study, the neutral disaccharides have functional groups completely protonated, while the deprotonated disaccharides are represented by removal of the hydrogen from the carboxylic acid groups to form charged carboxylate anions. The effects of deprotonated hydroxyl groups are not studied here due to their relatively high pK_a compared to the carboxylate groups ($\text{pK}_a = 3.4\text{-}4.4$) (Belitz and Grosch, 1987). However, the hydroxyls do play an important role in stabilization of the configurations of the disaccharides and respond to movements of the disaccharides, and especially act to stabilize the carboxylate groups by hydrogen bonding. Potential energy values in all plots are normalized with the lowest energy conformation as

$$E_{\text{plot}} = E_{\text{measured}} - E_{\text{minimum}} \quad (2)$$

for each of the disaccharides. Absolute potential energy values for each minimum are available in Table 4. The energetic contour plots of measured potential energies (kcal mol^{-1}) of protonated and deprotonated disaccharides at $\epsilon = 1$ and 78 provide the backgrounds of the figures highlighting dynamic molecular simulation (viz. Figures 3, 4, and 5) have not been included here as separate figures for brevity.

Table 4. Potential energy minima of torsional conformations of protonated and deprotonated alginic acid subunit disaccharides.

Disaccharide	Dielectric	Minimum	Φ (°)	Ψ (°)	E (kcal mol⁻¹)	ΔE^\ddagger (kcal mol⁻¹)
Protonated <i>MM</i>	1	<i>a</i>	306.0	240.0	7.88	0
		<i>b</i>	28.9	248.7	8.17	0.30
	78	<i>a</i>	290.6	241.1	23.74	0
		<i>b</i>	42.5	249.2	25.86	2.12
Deprotonated <i>MM</i>	1	<i>a</i>	279.0	226.3	73.38	0
	78	<i>a</i>	290.7	241.2	23.85	0
		<i>b</i>	41.3	249.1	26.54	2.69
Protonated <i>GG</i>	1	<i>a</i>	53.5	244.0	20.56	0
		<i>b</i>	289.8	233.4	26.04	5.48
		<i>c</i>	194.9	204.1	28.50	7.94
		<i>d</i>	236.2	59.2	31.96	11.39
	78	<i>a</i>	291.5	238.4	37.19	0
		<i>b</i>	37.3	250.1	39.27	2.08
Deprotonated <i>GG</i>	1	<i>a</i>	276.8	253.3	64.34	0
	78	<i>a</i>	284.6	223.1	26.38	0
		<i>b</i>	58.7	243.2	38.10	11.73
Protonated <i>MG</i>	1	<i>a</i>	292.1	242.7	13.15	0
		<i>b</i>	40.0	244.3	15.99	2.84
	78	<i>a</i>	291.5	228.3	25.88	0
		<i>b</i>	42.8	245.3	27.87	1.99
Deprotonated <i>MG</i>	1	<i>a</i>	299.5	225.1	76.03	0
	78	<i>a</i>	291.6	228.3	25.77	0
		<i>b</i>	42.3	244.6	28.25	2.47

$$\ddagger \Delta E = E_{\text{measured}} - E_{\text{minimum}}$$

MM disaccharides consistently exhibit two local minima in the torsion angle potential energy maps (Figures 3, 4, and 5), except when the disaccharide was deprotonated with $\epsilon = 1$ (Table 4). The global potential energy minimum (*a*) consistently was determined with an additional local minimum (*b*). Increasing the ϵ value causes a broadening of the minima for the protonated disaccharide. The deprotonated *MM* disaccharide appears to have only a single energy minimum at $\epsilon = 1$, while at $\epsilon = 78$ two local minima are observed. Presumably, the decreased torsional freedom at $\epsilon = 1$ results from interaction of the deprotonated carboxyl groups on the subunits. These interactions are electrostatically shielded when $\epsilon = 78$. The minimum *b* has a higher energy in this conformation because the carboxylates are axially eclipsed, that is, overlapping when examined along the long axis of the disaccharide, whereas they are equatorially oriented at minimum *a*. The eclipsing is more apparent at $\epsilon = 1$ with the deprotonated disaccharide where minimum *b* occurs at $\epsilon = 78$ because the unshielded nonbonded interactions result in high-energy conformations. This restriction does not occur with the protonated disaccharide due to the reduced charges associated with the functional groups.

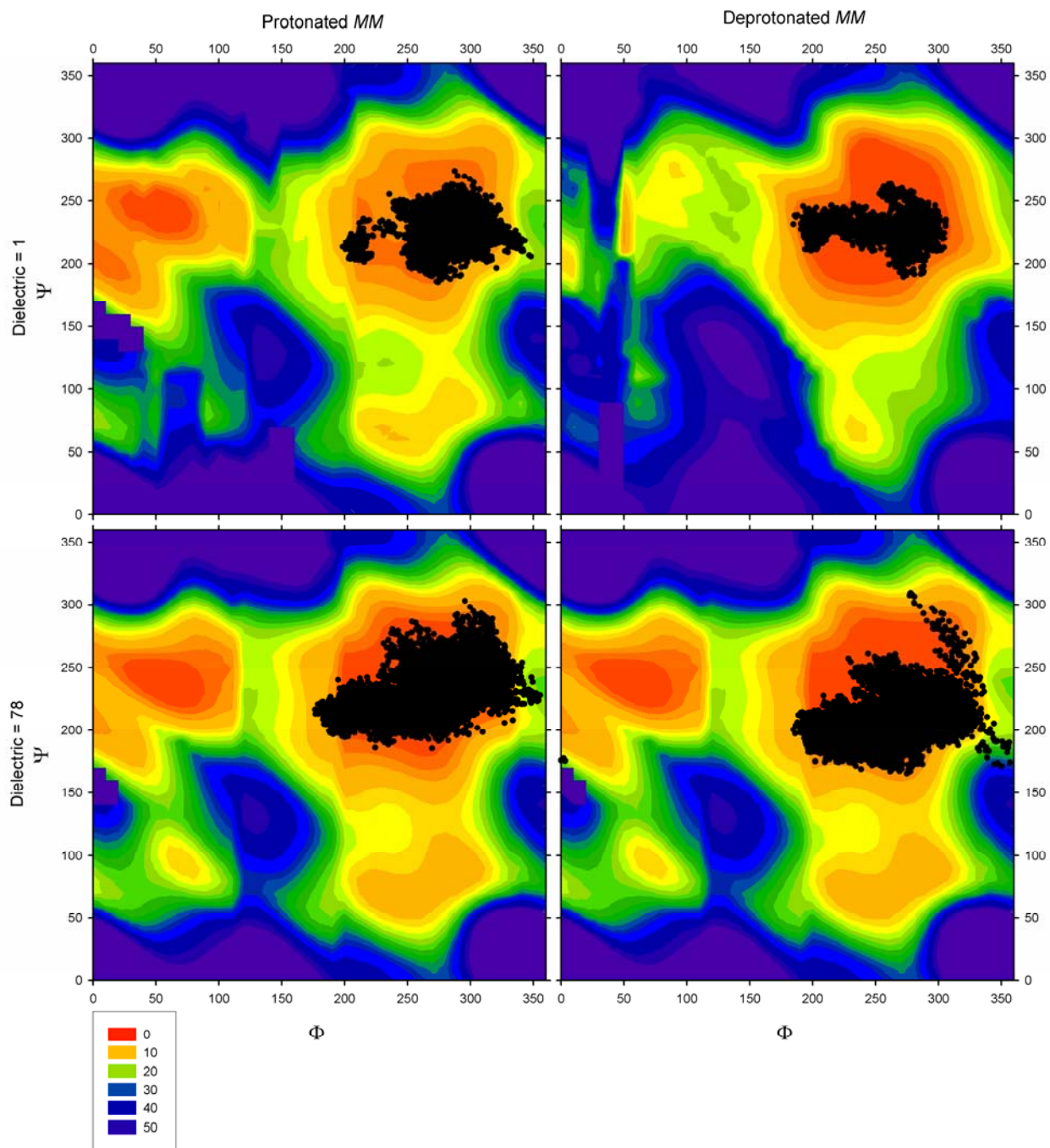


Figure 3. Molecular dynamic simulation (100 ps) of the torsional changes of protonated and deprotonated mannuronic disaccharides (*MM*) at 300 K superimposed over contour plots of the energy minima of the disaccharide. Contours are provided in kcal mol⁻¹.

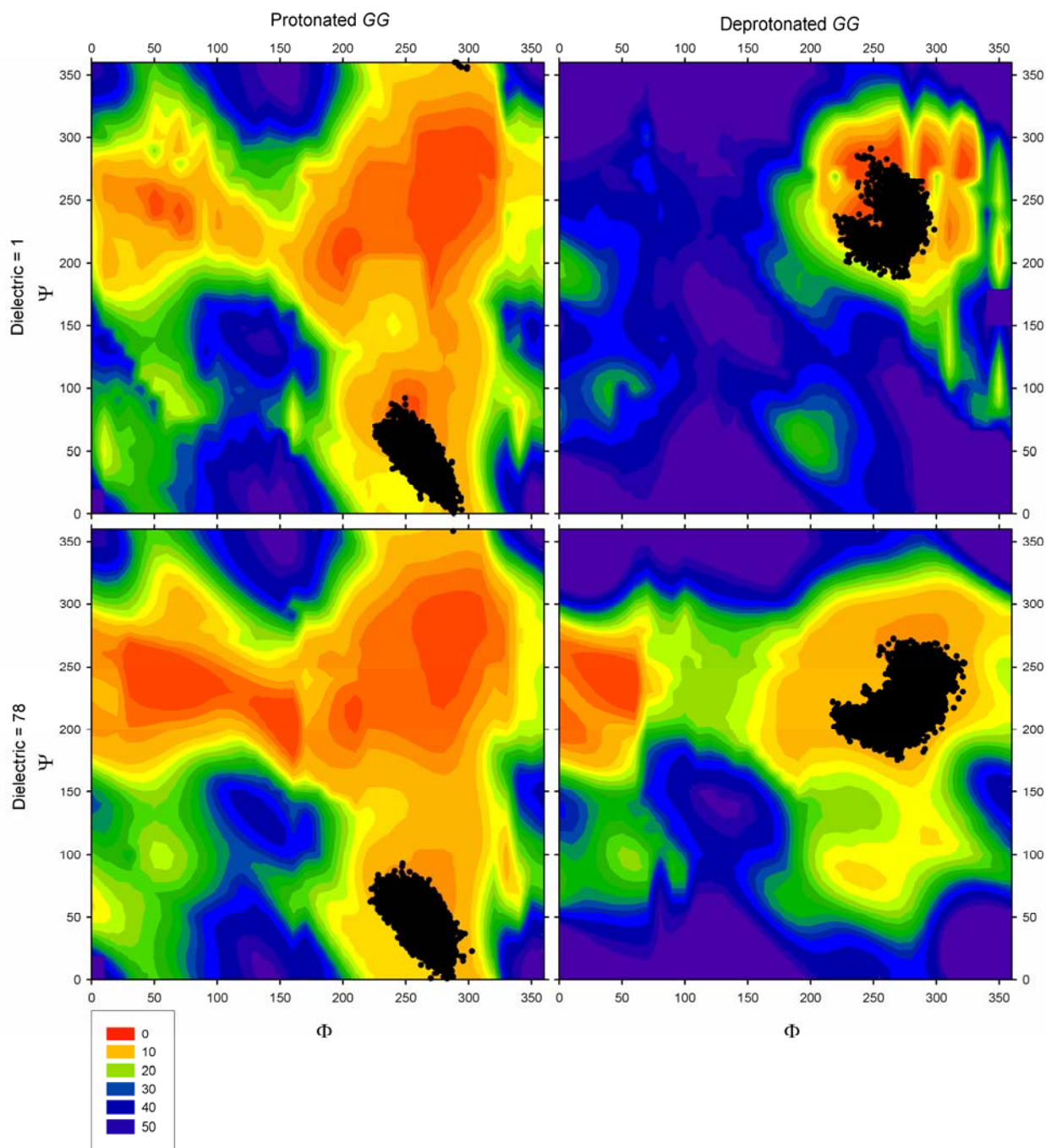


Figure 4. Molecular dynamic simulation (100 ps) of the torsional changes of protonated and deprotonated guluronic disaccharides (GG) at 300 K superimposed over contour plots of the energy minima of the disaccharide. Contours are provided in kcal mol⁻¹.

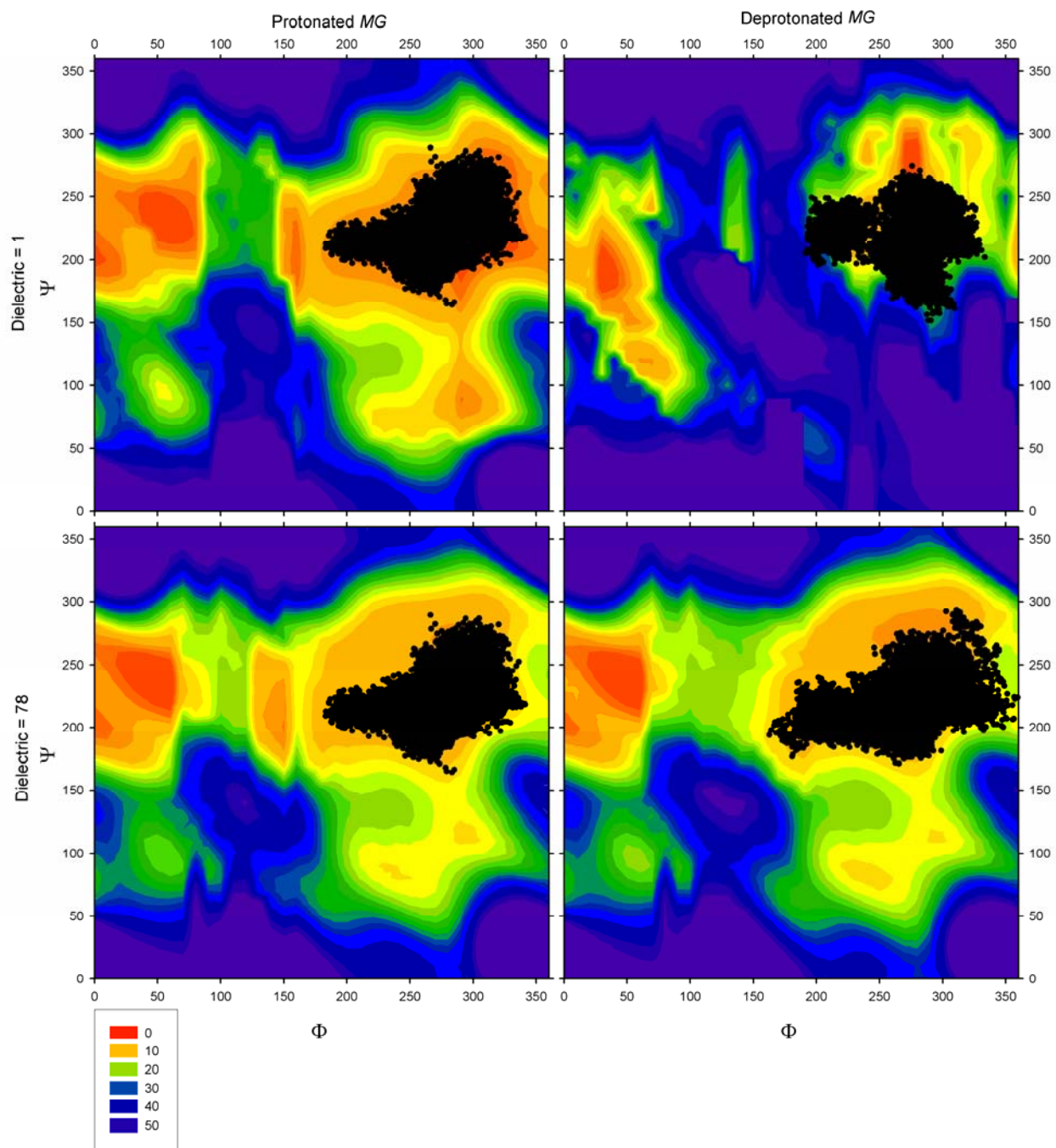


Figure 5. Molecular dynamic simulation (100 ps) of the torsional changes of protonated and deprotonated mannuronic/guluronic disaccharides (*MG*) at 300 K superimposed over contour plots of the energy minima of the disaccharide. Contours are provided in kcal mol⁻¹.

Torsion maps for the *GG* disaccharide exhibit minima in the same regions as the *MM* disaccharide. The protonated *GG* disaccharide at $\epsilon = 1$ exhibits a complex adiabatic map with four local minima (Table 4). The *GG* disaccharides have greater energy in all conformations than *MM* disaccharides (Table 4). This is likely due to their α -linkage and buckled conformation, which results in close association of interacting functional groups, in comparison to the more planar β -linkages of the *MM* disaccharides. *GG*-blocks are arranged in α -conformations with molecular repeats of 8.7 Å (Atkins et al., 1973a), while *MM* regions are β -linked with a 10.35 Å molecular repeat (Atkins et al., 1973b), and the close association of interacting functional groups is probably responsible for the reversal of the *a* and *b* minima in *GG* compared to the *MM* torsion maps. The deprotonated *GG* disaccharide at $\epsilon = 1$ exhibits extremely restricted torsional freedom due to the more closely spaced carboxylate groups in the α -linkage than in the β -linkage on the *MM* disaccharide, and hence more significant interactions of the eclipsing of negatively charged carboxylate groups. The α -conformation results in greater steric hindrance than the β -linked polysaccharides due to interaction of the oxygens on the carboxylate groups and decreased flexibility of the molecule (Whitting, 1971). Our findings on the torsional minima of *MM* and *GG* are in reasonable agreement with the conformations determined by Braccini et al. (1999).

The *MG* linkage exhibits similar torsional freedom as observed for the *MM* and *GG* disaccharides. When deprotonated with $\epsilon = 1$, the *MG* linkage has severely limited torsional freedom relative to the *MM* and *GG* disaccharides (Figure 5). The contrast in stabilization is less significant for the torsion maps calculated for $\epsilon = 78$ where the implicit solvation significantly reduces the intramolecular electrostatics for the charged carboxylate groups. Nonetheless, the mixed disaccharide exhibits similar Φ - Ψ mapping for the stable conformations at the *a* and *b* minima.

Comparison of the data for the disaccharides reveals interesting insights about the conformation of the disaccharides. For all disaccharides, except protonated *GG* with $\epsilon = 1$, the global energy minima *a* (i.e. the most stable confirmation) occurs at $\Phi \approx 270^\circ$, $\Psi \approx 240^\circ$, while the second most stable confirmation appears at $\Phi \approx 45^\circ$, $\Psi \approx 245^\circ$ (Table 4). Deprotonated disaccharides are stabilized by 15 – 20 kcal mol⁻¹ with increasing ϵ (Table 4) due to shielding of the Coulombic interactions associated with the carboxylate groups. In contrast, raising ϵ destabilizes protonated disaccharides, as demonstrated by increased potential energy values. The α -linked disaccharides generally have higher potential energy values than the more planar β -linked disaccharides because of the closer spatial arrangement of interacting functional groups and increased destabilizing interactions. The *MG* linkage can exhibit energetics similar to *GG* or *MM* linkages depending on the torsional conformation the disaccharide. The most stable conformation of Ψ among all monosaccharide constituents occurs near a torsional conformation of 240° . This defining feature is attributed to the positioning of the carboxylate carbon (C_1) away from the ether linkage on the Ψ -linkage (viz. Figure 1) as opposed to two carbons away on the Φ -linkage and the restricted torsional freedom controlled by this dominant functionality closely interacting with the adjacent monosaccharide. In order to better assess the stability of the various disaccharide configurations at ambient conditions and to observe any temporal variation, molecular dynamic simulations were conducted.

3.2. Molecular Dynamics Simulations with Disaccharides

Molecular dynamics simulations demonstrate that *MM*, *GG*, and *MG* disaccharides are most stable near the global energy minimum (*a*) for all protonated and deprotonated disaccharides at $\epsilon = 1$ and 78, excluding the protonated *GG* disaccharide. Starting conformations for these simulations were derived from minimized disaccharide structures with chiral centers that were empirically shown to be part of a naturally produced polymer.

The initial configuration for the *MM* linkage is at $\Phi = 206.7^\circ$, $\Psi = 217.3^\circ$. For all simulations, the disaccharide maintains its position in the potential energy trough associated with minima *a* (Figure 3). There is some oscillation of the torsion values within the trough associated with the energy minimum. The occasional blocking at potential energy barriers for certain conformations (e.g. protonated *MM*, $\epsilon = 1$, $\Phi = 0-30^\circ$, $\Psi = 150^\circ$) is the result of an energetically unfavorable conformation resulting in nonconvergence of the energy minimization calculations and data smoothing assumptions made while plotting.

Protonated *GG* disaccharide simulations were initiated with $\Phi = 266.0^\circ$, $\Psi = 38.9^\circ$ (Figure 4). This conformation represents the structure reported in several empirical studies investigating natural alginate. Upon deprotonation, this conformation changes to the starting position $\Phi = 276.8^\circ$, $\Psi = 253.3^\circ$ (Figure 4) due to the interaction of carboxylate groups, and represents the more likely *in situ* conformation because of the low pK_a of the carboxylate group. Deprotonated *GG* disaccharides exhibited a similar conformational preference associated with minimum *a* as observed for *MM* disaccharides (Figure 4) and the disaccharides similarly explored energy troughs about their minimum energy conformations. It is significant to note that the protonated *GG* disaccharide did not have sufficient energy at 300 K to move from the local minimum *d* to the global minimum *a*.

MG disaccharide simulations began at $\Phi = 301.2^\circ$, $\Psi = 235.3^\circ$, and further demonstrate the stability of the preferred molecular arrangement associated with global minimum *a* (Figure 5). The *MG* disaccharide exhibits movement to higher energy levels at 300 K than demonstrated by *MM* and *GG* disaccharides. This greater variation in torsion angle results from the higher energy, and, therefore, least stable minima of *MG* disaccharides in comparison with the *MM* or *GG* disaccharides (Table 4).

To demonstrate the effect of initial torsion angle configuration on disaccharide conformation, molecular dynamics simulations were also run with protonated *MM* and *GG* disaccharides, $\epsilon = 1$ (Figure 6), but starting with a configuration corresponding to the local minimum *b* (*MM*: $\Phi = 50.0^\circ$, $\Psi = 243.0^\circ$; *GG*: $\Phi = 59.0^\circ$, $\Psi = 242.0^\circ$). The results show that both *MM* and *GG* disaccharides evolve from the local minimum *b* to the global minimum *a*, indicating that at 300 K there is an energetic preference for transition to the stable conformation at minimum *a*. The potential energy surface exhibits an increased breadth of the trough and relatively low energy barrier to ease the transition through this saddle point. Comparison of these dynamics results to those for the protonated *GG* (viz. Figure 4) demonstrate that this barrier is lower than the energy barrier for conformational shift from minima *d* to *a*. Presumably, with enough thermal energy the molecule should be able to surpass this energy barrier and achieve conformation *a*.

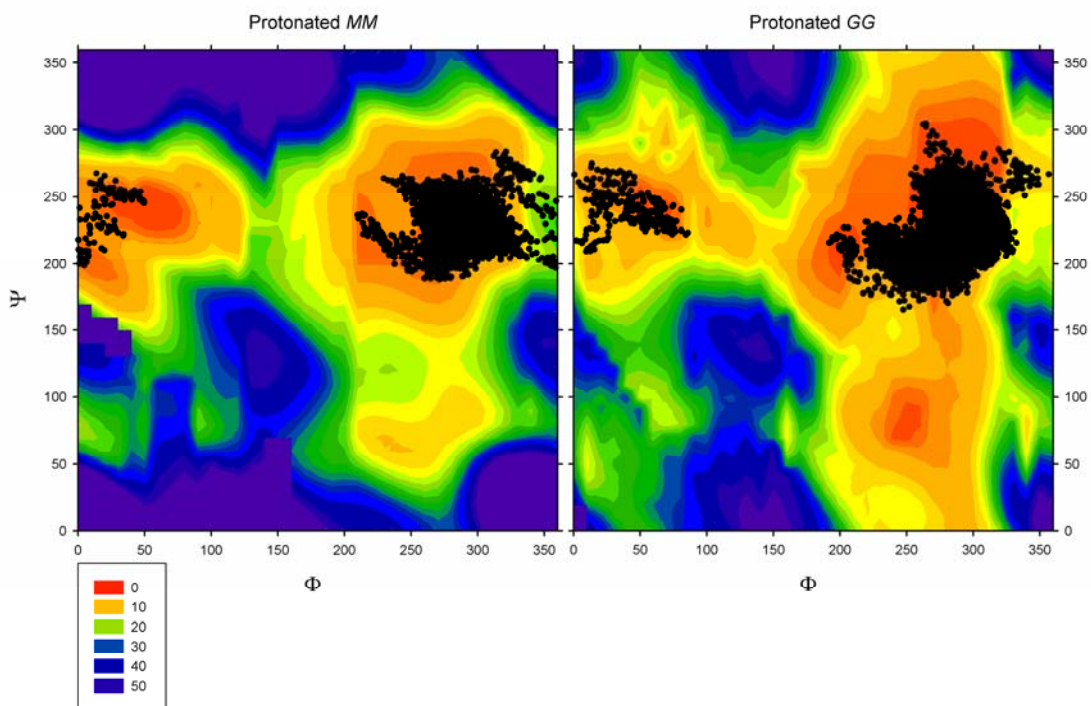


Figure 6. Molecular dynamics simulation (100 ps) of protonated mannuronic and guluronic disaccharides started at the local minimum *b* at 300 K, $\epsilon = 1$. Contours are provided in kcal mol⁻¹.

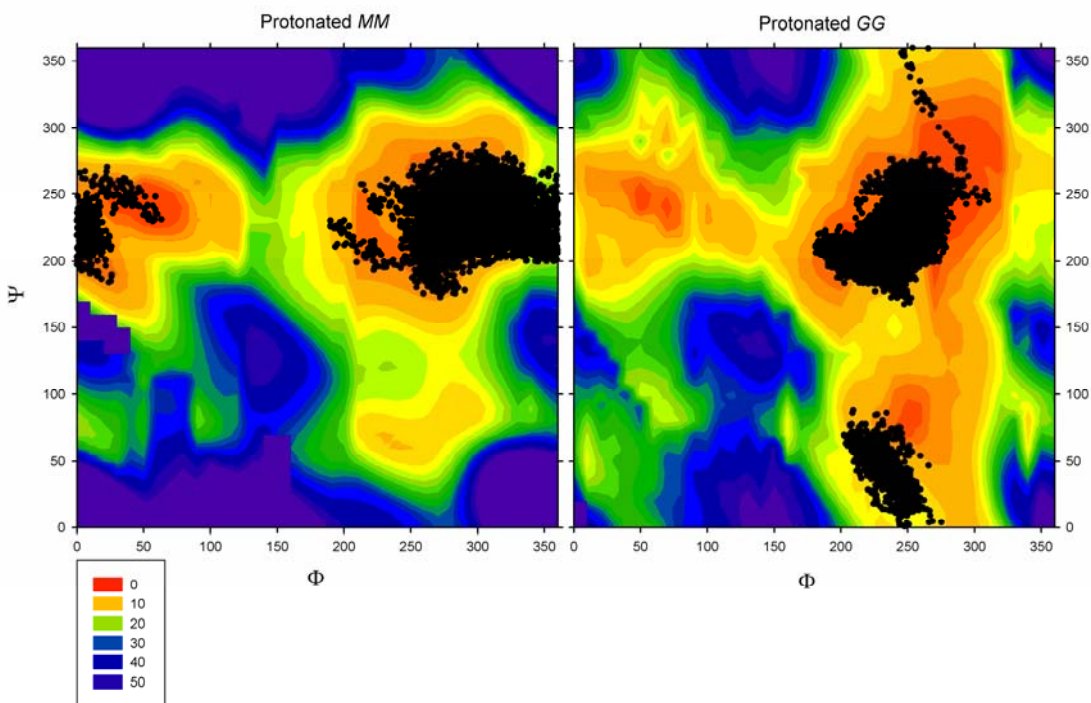


Figure 7. Molecular dynamics simulation (100 ps) of protonated mannuronic (*MM*) and guluronic (*GG*) disaccharides at 400 K, $\epsilon = 1$, started at the local minima *b* and *d*, respectively. Contours are provided in kcal mol⁻¹.

To assess the significance of the energy barrier, simulations were performed at 400 K with the original starting configurations of *MM* and *GG* disaccharides (Figure 7). Indeed, after occupying minimum *d*, the *GG* disaccharide proceeds to the configuration represented at minimum *a*. However, these simulations do not indicate any preference, temporary or otherwise, of the disaccharide for the local minimum *b* conformation. In contrast, the additional thermal energy allows the *MM* disaccharide to move relatively freely between configurations represented by minima *a* and *b*, indicating that this barrier is lower for the *MM* disaccharide than for the *GG* disaccharide.

Based on the molecular dynamics simulation results represented in Figures 3-7, the expected variation in the torsion linkages of alginic acid disaccharides are evaluated (Table 5). Independent of starting conformation, the preferred conformation of disaccharides is primarily associated with the global potential energy minimum *a*.

Table 5. Torsional variation of protonated and deprotonated alginic acid disaccharides during dynamic simulation.

<i>Disaccharide</i>	Φ (°)	Ψ (°)
Protonated <i>MM</i>		
$\epsilon = 1$	288.3 ± 16.3	227.7 ± 10.5
$\epsilon = 78$	274.5 ± 31.6	233.7 ± 17.3
Deprotonated <i>MM</i>		
$\epsilon = 1$	258.6 ± 30.7	227.1 ± 11.4
$\epsilon = 78$	274.5 ± 31.6	233.7 ± 17.3
Protonated <i>GG</i>		
$\epsilon = 1$	260.8 ± 9.5	44.8 ± 13.8
$\epsilon = 78$	257.5 ± 11.4	49.8 ± 12.6
$\epsilon = 1^*$	274.2 ± 19.6	225.0 ± 19.4
Deprotonated <i>GG</i>		
$\epsilon = 1$	266.3 ± 14.4	234.7 ± 19.1
$\epsilon = 78$	276.7 ± 17.1	222.8 ± 17.9
Protonated <i>MG</i>		
$\epsilon = 1$	278.5 ± 29.1	226.4 ± 20.0
$\epsilon = 78$	278.2 ± 29.0	226.1 ± 19.9
Deprotonated <i>MG</i>		
$\epsilon = 1$	276.4 ± 28.0	219.9 ± 20.4
$\epsilon = 78$	270.8 ± 35.0	221.9 ± 19.9
<i>Average</i> [†]	274.1 ± 7.2	227.2 ± 4.8

*Simulation performed at 400 K. Statistics performed after molecule stabilized at local minimum B (viz. Figure 7).

[†]Excludes protonated *GG* simulations conducted at 300 K.

3.3. Molecular Dynamics Simulations with Polymers

To extend the two-unit models to polymers, alginic acid disaccharides *MM* and *GG* were repeated to form initial twenty-unit polysaccharide models, configured with bond geometry corresponding to the simulated global energy minimum. Molecular dynamics simulations performed at 300 K provide trajectories for the equilibrated polymers that further reinforce the stability associated with the torsional geometry characterized by the potential energy trough at minimum *a* (Figure 8). Some polymer linkages appear to access other minima regions and may be stabilized by intramolecular interactions throughout the polymer chain. Access of these other minima regions may represent the mechanism of stabilizing conformations associated with kinks or bends in the linear polymer chain. Temperature does not greatly affect the conformation of the polymers in terms of torsional access to the other minima regions (Figure 9). In fact, increasing the temperature for simulations to 400 K appears to constrain the polymeric linkages around minimum *a*, although there is increased Φ - Ψ variation within the energy trough. This result may be due to the increase in intrapolymeric interactions that favor a straight-chain conformation. The only exception is a single linkage on the *G*-polymer, which may be the result of a significant bend in the polymer creating greater intramolecular nonbonded interactions.

3.4. Association of Calcium Ions with Disaccharides and Polymers

The previous simulations are necessary for developing a baseline understanding of the effects of structural conformation and configuration on the three-dimensional form of alginic acid subunits. However, these polysaccharides are likely associated with charged cations *in situ*. The cations act to stabilize otherwise unfavored conformations. To assess the relative stability of cation binding by different conformations and configurations of disaccharides, calcium ions were manually docked with the previously determined energy minimized structures of deprotonated disaccharides and then subsequently energy minimized without any atomic or geometry constraints (Figure 10). The proximity of oxygen electron-donating moieties to calcium during chelation by deprotonated alginic acid disaccharide units and the effect on torsion and relative stability are summarized in Table 6. E_{Total} was calculated as in eq (1) for the entire simulation system including the calcium ion and the binding energy (E_{Bind}) was calculated as follows:

$$E_{Bind} = E_{Total\{Ca^{2+}\text{-dimer}\}} - E_{Total\{dimer\}} \quad (3)$$

The results indicate strong binding of the calcium ion by the all the representative disaccharides. However, binding and complex stability vary, depending on torsion angles, from the optimum values associated with minimum *a* in some cases (Braccini and Pérez, 2001). For example, the *MM* disaccharide appears to have the greatest stability when binding calcium in a conformation associated with the minimum *b* (Table 6, Figure 10). The *GG* disaccharide has two stable conformations when associated with calcium near the minimum *a*. The conformations varied depending on the localization of the calcium with the disaccharide, i.e. placement near to or far from the disaccharide-linkage ether (Emmerichs et al., 2004). Interestingly, near association with the disaccharide-linkage ether is a more energetically favorable state, presumably due to the closer association with stabilizing oxygens. Additionally, the *GG* disaccharide will not maintain a conformation corresponding to minimum *b* and instead favors a conformation reminiscent of

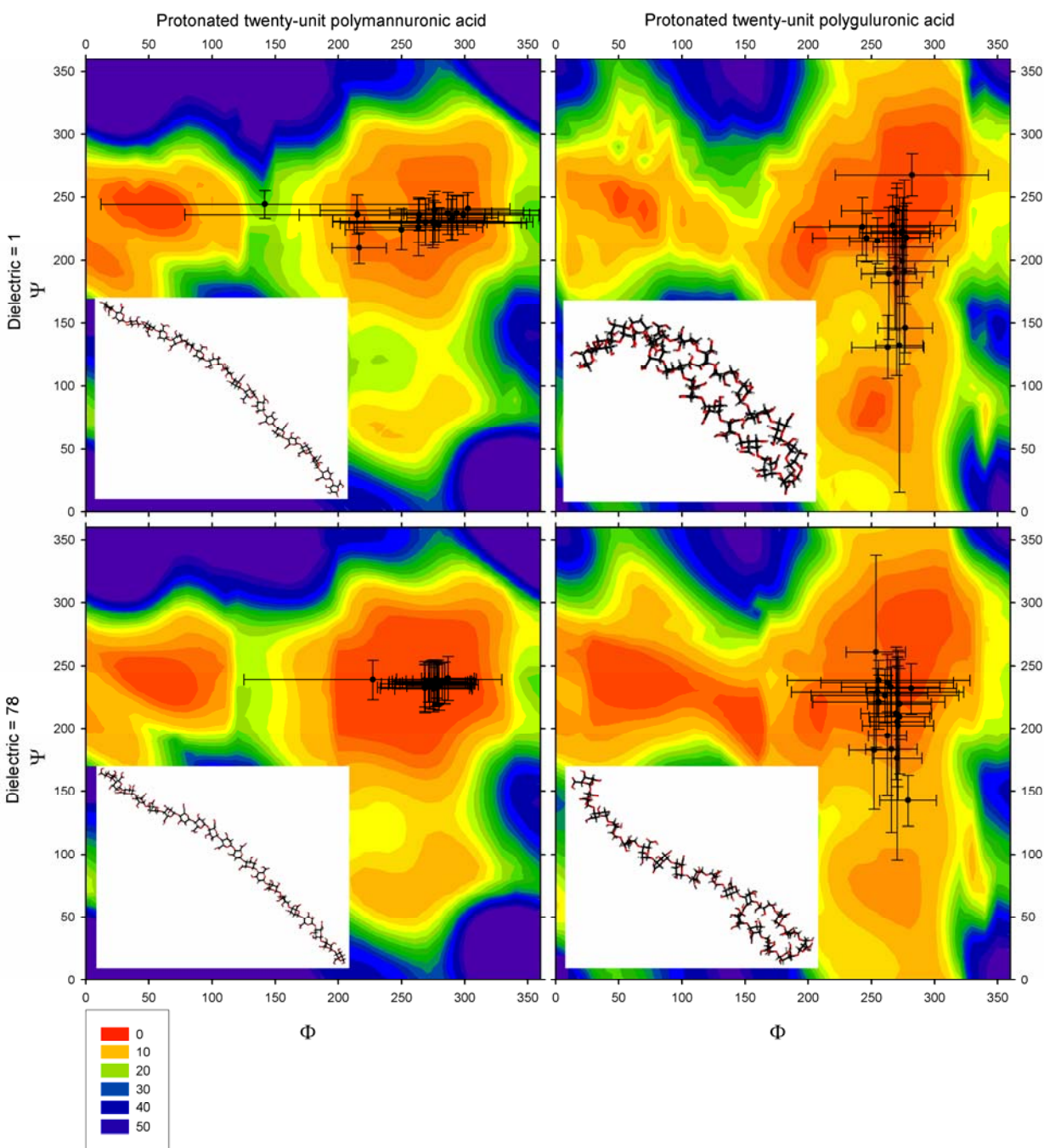


Figure 8. Molecular dynamics simulation of polysaccharides consisting of twenty units at 300 K. Each data point represents a single ether linkage and error bars represent one standard deviation in the torsional states experienced by that bond. The final configuration of the simulations is shown in the insets. Contours are provided in kcal mol⁻¹.

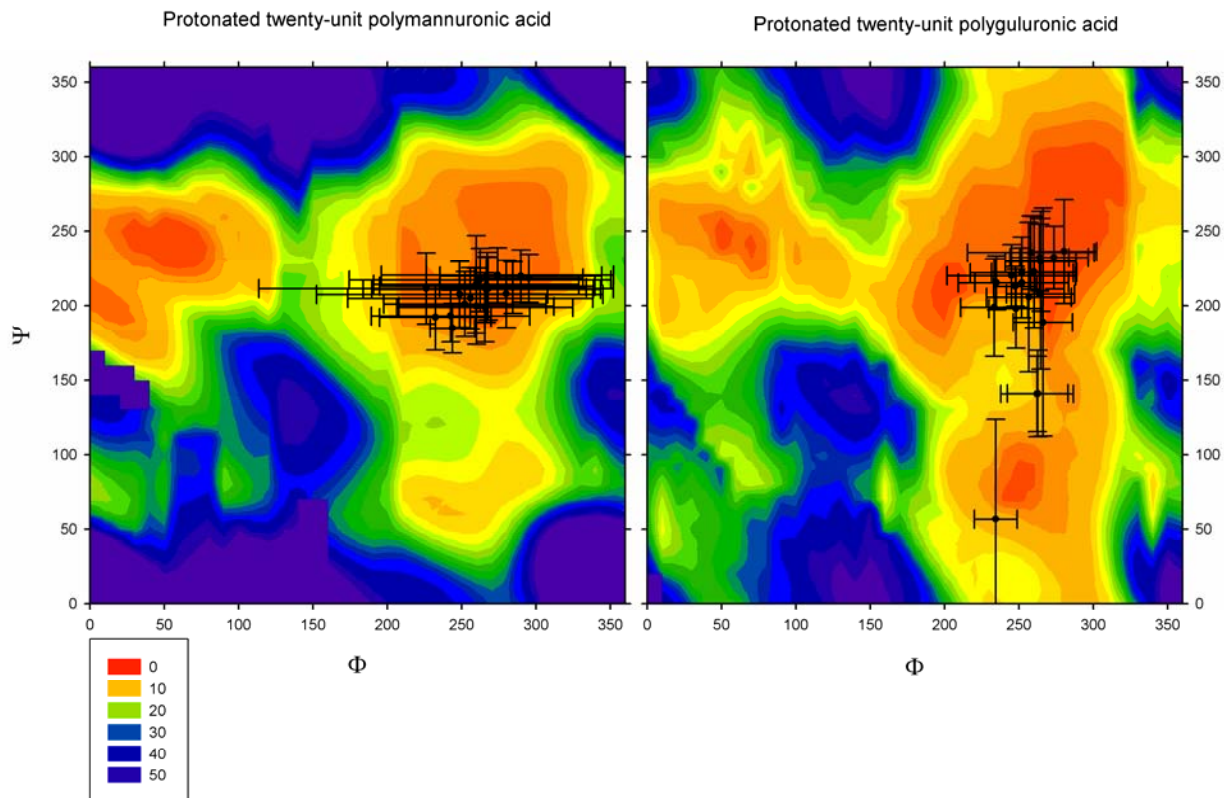


Figure 9. Molecular dynamics simulation of polysaccharides consisting of twenty units at 400 K and $\epsilon = 1$. Each data point represents a single ether linkage and error bars represent one standard deviation in the torsional states experiences by that bond. Contours are provided in kcal mol^{-1} .

minimum d in simulations at $\epsilon = 1$ with protonated GG . MG disaccharides exhibit stable conformations associated with minima a and b . When associated with calcium, these disaccharides also are stable in a conformation reminiscent of minimum c in simulations at $\epsilon = 1$ with protonated GG , indicating the α -linkage of this disaccharide may play a significant role in development of stable cation complexes (Latner et al., 2003). The Coulombic energy stabilization gained by the formation of a relatively strong Ca^{2+} -carboxylate coordination in all disaccharides easily offsets the destabilization introduced by transients in the Φ - Ψ angles. The exact energy gain also needs to include the hydration energy of a calcium ion in solution.

To assess polymer binding of cations, energy-minimized disaccharides associated with calcium ions were used to construct polymer models, which were subsequently energy minimized (Figure 11). The total potential energies of the polymer-calcium complexes are (kcal mol^{-1}): $MM-a = -3784.25$, $MM-b = -3931.81$, $GG-a = -3381.18$, $GG-a_2 = -3214.85$, $GG-d = -4153.95$, $MG-a = -4066.20$. MM and MG polymers were significantly less buckled than GG polymers. All polymers were stabilized by Coulombic interactions, which allowed for increased bond strain (e.g. $MG-a$). Further stabilization of the polymers is expected with the addition of extra polymer chains to form polymeric bundles and extended two dimensional structures. However, these

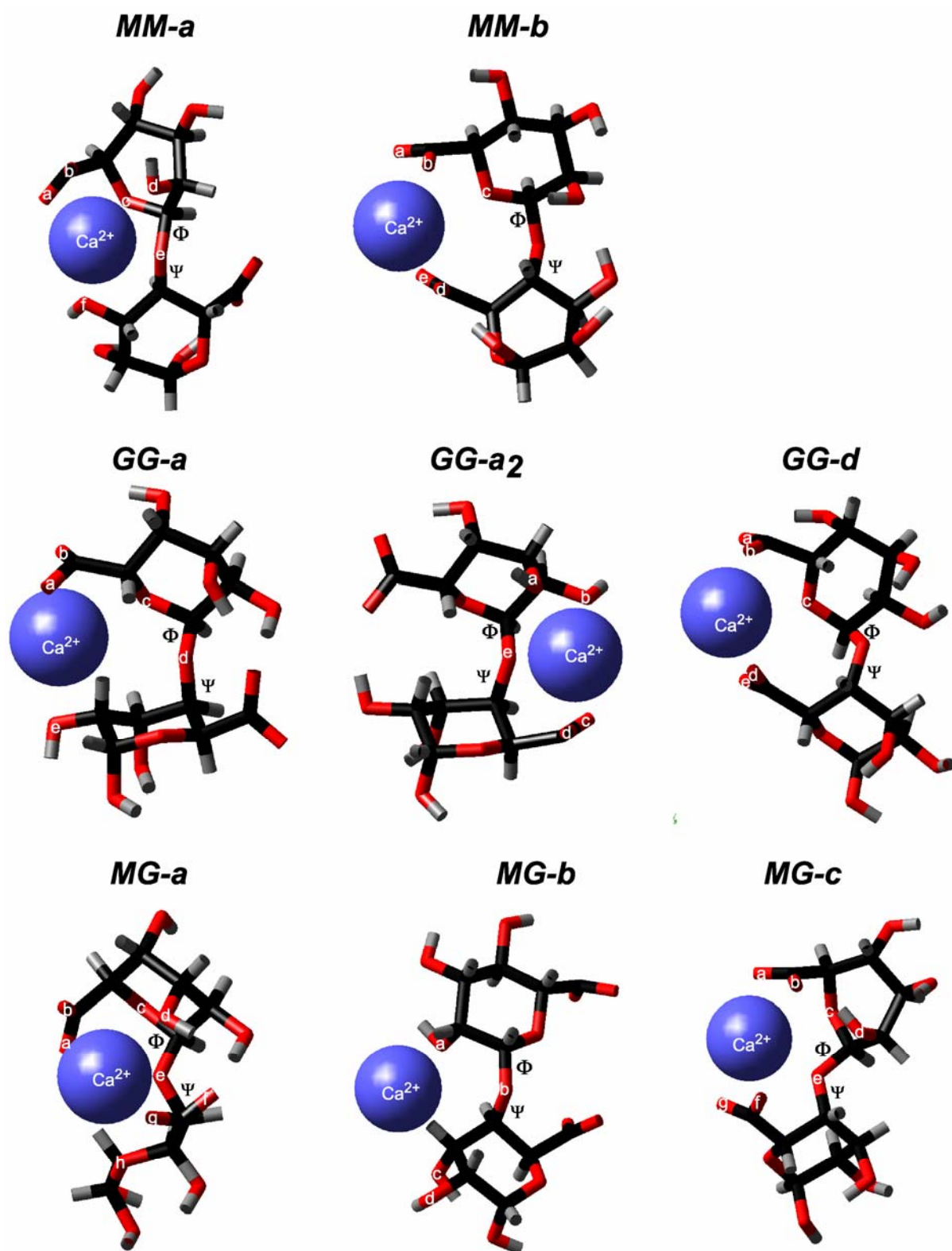


Figure 10. Energy-minimized structures of alginate subunit disaccharides associated with calcium ions. Data for oxygen-calcium distance, bond torsion, and binding and total energies are presented in Table 6. Color key: black = carbon, red = oxygen, gray = H, blue = calcium.

Table 6. Proximity of oxygen electron-donating moieties to calcium during chelation by deprotonated alginic acid disaccharide units and the effect on torsion and relative stability.

Distance to Ca ²⁺ (Å)	<i>MM-a</i>	<i>MM-b</i>	<i>GG-a</i>	<i>GG-a₂</i>	<i>GG-d</i>	<i>MG-a</i>	<i>MG-b</i>	<i>MG-c</i>
<i>a</i>	2.39	2.35	2.39	2.39	2.36	2.34	2.95	2.31
<i>b</i>	2.36	2.34	2.32	2.42	2.44	3.34	3.43	2.34
<i>c</i>	2.65	3.00	2.84	2.60	2.58	3.84	3.52	3.55
<i>d</i>	2.66	2.29	3.77	2.30	2.28	2.50	3.72	3.67
<i>e</i>	2.35	2.80	2.56	3.38	2.30	2.51	-	2.79
<i>f</i>	2.42	-	-	-	-	3.30	-	2.34
<i>g</i>	-	-	-	-	-	2.27	-	2.30
<i>h</i>	-	-	-	-	-	2.63	-	-
Φ (°)	282.3	44.8	247.1	275.1	267.4	212.3	69.7	187.1
Ψ (°)	258.6	246.7	204.2	192.5	13.5	209.6	236.5	174.8
E_{Bind} (kcal mol ⁻¹)	-412.60	n.d.	-367.64	-403.68	n.d.	-499.64	n.d.	n.d.
E_{Total} (kcal mol ⁻¹)	-338.86	-412.80	-303.30	-339.35	-410.10	-423.61	-416.64	-412.67

n.d. = not determined

complex structures are beyond the present scope of the investigation and will need to be addressed in a future study.

The conformation and configuration of alginic acid disaccharides and polymers have been shown to be important in molecular energy stability, with a similar global energy minimum conformation for all representative subunits. These conformations are favored in polymers, as well, but intramolecular stabilization allows limited exploration of less-favored conformations. The simulations demonstrate that Coulombic stabilization by cations is a determining factor for disaccharides to stabilize at other conformations than those determined bonded energy terms. Torsional states experienced by disaccharides associated with calcium are significantly different from the global energy minimum. The greater stabilization effect is apparent when modeling cations with polymers where cations can be observed interacting with several monosaccharides (Figure 11).

3.5. Simulations with Alginic Acid Disaccharides and the (10 $\bar{1}$ 4) Calcite Face

Molecular dynamic simulations were performed to determine the role of conformation of alginic acid subunits on sorption to the (10 $\bar{1}$ 4) calcite surface. The disaccharides are initially positioned in the simulation cell and allowed to interact with the surface and in solution in two conformations: the global energy minimum (*a*) and a local energy minimum (*b*), as previously determined. The disaccharides are compared as aqueous species and surface-sorbed complexes (viz. Figure 2). The most stable orientation and binding distance to the calcite surface for each disaccharide were systematically determined before performing the simulations. The sorption energy is determined by taking the difference of the potential energy of the simulation cells (eq.

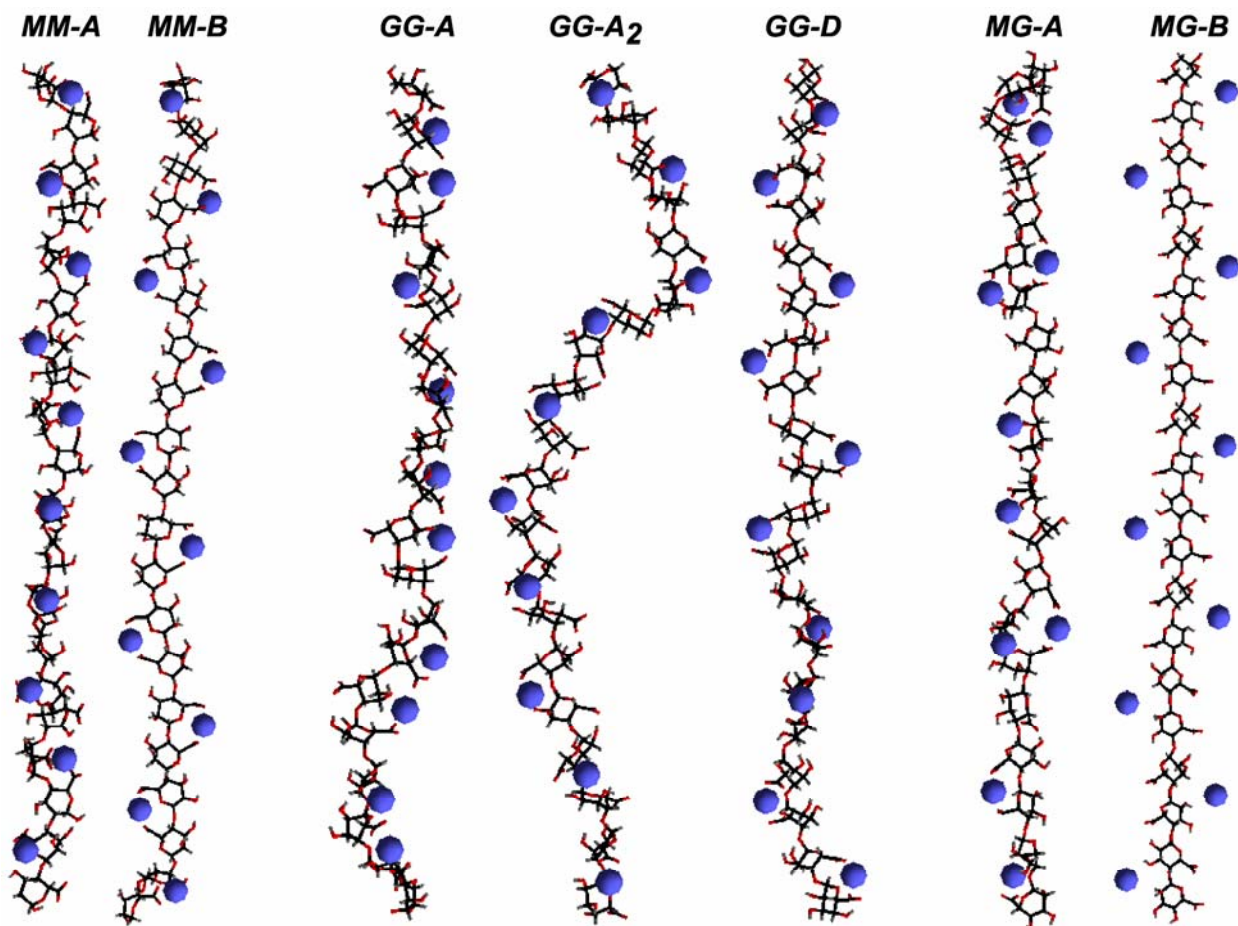


Figure 11. Energetically minimized structures of polymers in different torsional conformations corresponding to different starting positions of torsional energy minima associated with calcium ions localized in potential chelation sites. Color key: black = carbon, red = oxygen, gray = H, blue = calcium.

1) for the two different positions of the disaccharide within the simulation cell. This approach provides a convenient alternative for evaluating the sorption enthalpy since the simulation cells are identical except for the placement of the molecule. Hence, any differences in the energy values are the result of the disaccharide interactions with the solvating water molecules and with the calcite surface. However, it is important to note that the energy determinations are useful for relative comparison of the systems but should not be considered comparable to absolute or *in situ* energies. Molecular dynamics simulations were conducted and analyzed for all the representative disaccharides. The results are provided in Table 7 and Figure 12. As noted previously, only a detailed account of the relevant chemistry for the *GG* disaccharide is presented; similar phenomena to those described in the following sections control the energetics of the other disaccharides.

The surface-sorbed (surficial) configuration for each of the disaccharides is found to be the more stable (Figure 12A) of the two simulations and sorption is exothermic (de Leeuw and Cooper,

Table 7. Torsional variation of the ether linkage during 50 ps molecular dynamic simulations for solvated and sorbed (calcite (10 $\bar{1}$ 4) surface) disaccharides.

Disaccharide	$\Phi \pm$ Standard Deviation ($^{\circ}$)			$\Psi \pm$ Standard Deviation ($^{\circ}$)		
<u>GG</u>						
<i>a</i> Starting Conformation [†] :						
$\Phi \sim 256, \Psi \sim 233$						
Solvated	223.4	\pm	10.5	216.3	\pm	7.4
Surficial	274.5	\pm	8.0	274.0	\pm	6.6
<i>b</i> Starting Conformation [‡] :						
$\Phi \sim 61, \Psi \sim 284$						
Solvated*	280.0	\pm	18.9	258.3	\pm	24.0
Surficial	51.0	\pm	7.1	269.8	\pm	7.2
<u>MG</u>						
<i>a</i> Starting Conformation [†] :						
$\Phi \sim 290, \Psi \sim 231$						
Solvated	268.0	\pm	9.5	206.4	\pm	14.0
Surficial	280.6	\pm	9.8	271.3	\pm	6.7
<i>b</i> Starting Conformation [‡] :						
$\Phi \sim 70, \Psi \sim 230$						
Solvated*	201.3	\pm	9.4	220.3	\pm	9.3
Surficial	36.0	\pm	6.9	238.8	\pm	6.0
<u>MM</u>						
<i>a</i> Starting Conformation [†] :						
$\Phi \sim 197, \Psi \sim 221$						
Solvated	196.0	\pm	11.6	221.9	\pm	10.6
Surficial	262.1	\pm	8.5	214.4	\pm	7.2
<i>b</i> Starting Conformation [‡] :						
$\Phi \sim 52, \Psi \sim 225$						
Solvated*	277.5	\pm	15.3	229.7	\pm	12.5
Surficial	218.6	\pm	**	193.0	\pm	**

[†]*a*: global energy minimum

[‡]*b*: local energy minimum

*Note: During equilibration (initial 20 ps) these simulations have shifted to the *GM* conformation (viz. Figure 15).

**Torsional values are the final values recorded from the 20 ps equilibration simulation (due to instabilities in the production simulation).

2004). The solvated forms of the disaccharides all exhibit a higher potential energy because of, in part, the charged carboxylate groups. Interaction of the disaccharides with the surface allows localization of the negatively charged carboxylates and the positively charged calcium ions at the mineral surface. The sorption energies of the disaccharides were calculated to compare the magnitude of the interaction of the different disaccharides with the calcite surface (Figure 12B). The disaccharide-conformation of *GG-a* is significantly more stable on the calcite surface and is

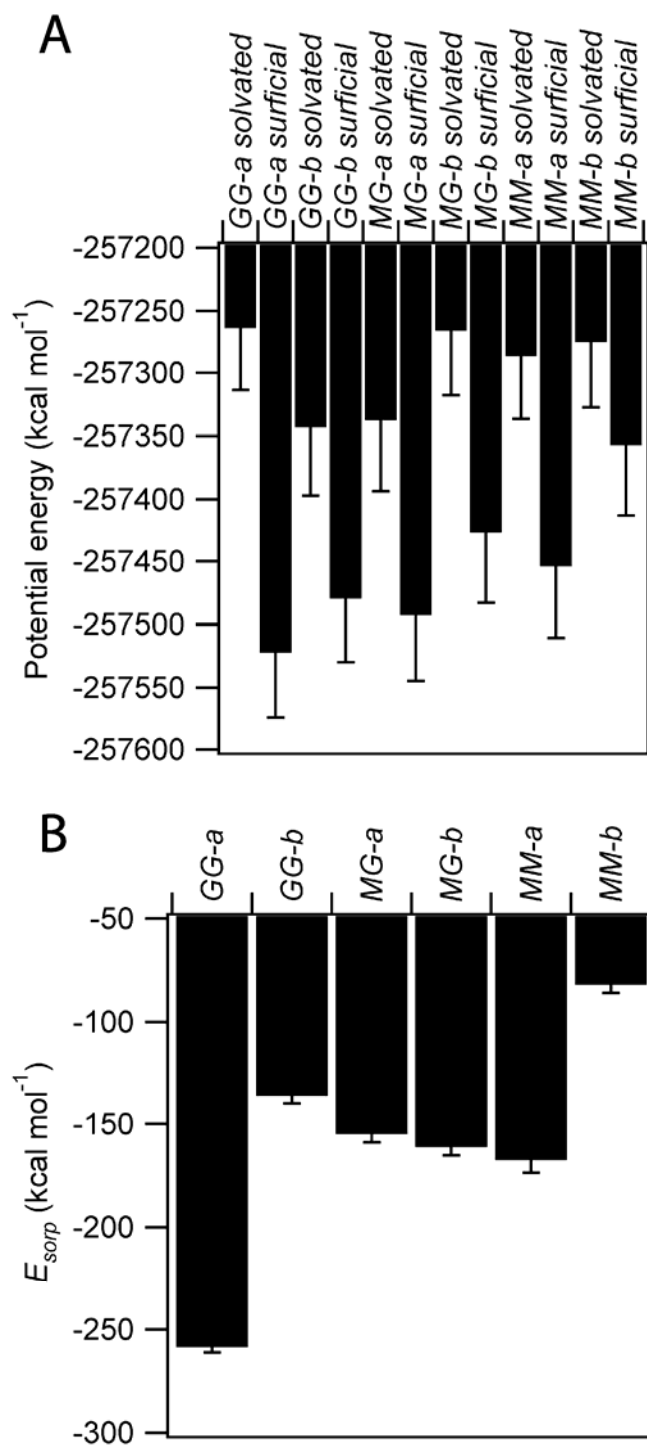


Figure 12. Average potential energy (\pm standard deviation) of the simulation cells (A) and the disaccharide sorption energy (B) derived from the 50 ps production simulations. *MM-b* data is recorded from the 20 ps equilibration run due to instabilities in the 50 ps production run.

stabilized by approximately 250 kcal mol⁻¹. The *GG* disaccharide has been experimentally demonstrated to form stronger interactions with aqueous cations due to the appropriate spacing and configuration of cation-stabilizing moieties. It is likely that the same features allow the disaccharide to strongly interact with the cations on the calcite surface. The *MG-a* and *-b* disaccharides also formed stable associations with the calcite surface. Although *GG*-blocks have consistently been reported as the chelating portion of alginic acid, *MG*-blocks have recently been implicated as being able to bind aqueous cations (Lattner et al., 2003).

The differences in the sorption energies of the *GG-a* and *GG-b* disaccharides indicate that there is significant conformational control of disaccharide interaction by the calcite (10 $\bar{1}$ 4) surface. These two disaccharides are chemically identical and differ only in their starting torsional arrangements. The role of conformation on localization of the active sorption moieties of the disaccharides was compared for the *a* and *b* conformations of *GG*.

The conformations of the *GG* disaccharides control interaction of the electron-donating moieties with the cations of the surface (Figure 13) (Emmerichs et al., 2004). Contour plots of the density of the actively-binding atoms derived from the trajectories demonstrate that the *GG-a* disaccharide interacts with the surface with one carboxylate group, two ether oxygens, and several hydroxyls. The *GG-b* disaccharide interacts with a single carboxylate, a single ether oxygen, and multiple hydroxyls. An important difference in the two arrangements is the disposition of the ether oxygen associated with the ring linkage (>C-O-C<). In the *GG-a* form, the ether oxygen linking the monosaccharides is in close proximity to the calcite surface, whereas in the *GG-b* form the ether oxygen is situated up and away from the surface. The additional stabilization provided by the interaction of this relatively immobile ether oxygen, in comparison to hydroxyls, appears to substantially affect the sorption energy.

The relative importance of the various electron-donating portions of the disaccharides is quantified by measuring the radial distribution functions (RDF) for Ca-O interactions, specifically for the oxygen atoms in the disaccharides and the calcium atoms in the first surface layer of the calcite (Figure 14). The ether oxygens on the *GG-a* disaccharide interact most strongly with the calcite surface as characterized by the dominant RDF peak at 3.6 Å, whereas for the *GG-b* disaccharide the equivalent RDF is significantly diminished. On the *GG-b* disaccharide, the hydroxyls appear to be the dominant interacting moieties as indicated by the main peak that is centered at 3.7 Å. However, the relative freedom of these atoms in comparison to the ether oxygens results in a less controlled association, as evidenced by the substantial breadth of this Ca-O RDF peak.

Simulations having the disaccharides initially in the local potential energy conformation (*b*) all reverted to the global energy minimum (*a*) during the equilibration simulations. The solvated *GG-b* disaccharide quickly (within several picoseconds) transformed into the global energy minimum (*a*) conformation during the preproduction equilibration simulation (Figure 15). An analysis of the variation in the two torsion angles (Ψ and Φ) and associated with the disaccharide ether linkage provides a good metric for this transformation. It appears that at 0.1-0.9 ps, the torsion angle Ψ varies to allow rotation of torsion angle Φ about the -C-O- bond, after which both torsion angles reequilibrate to the stable conformation associated with the global energy minimum (*a*). The coordinated rotations result in a potential energy stabilization of

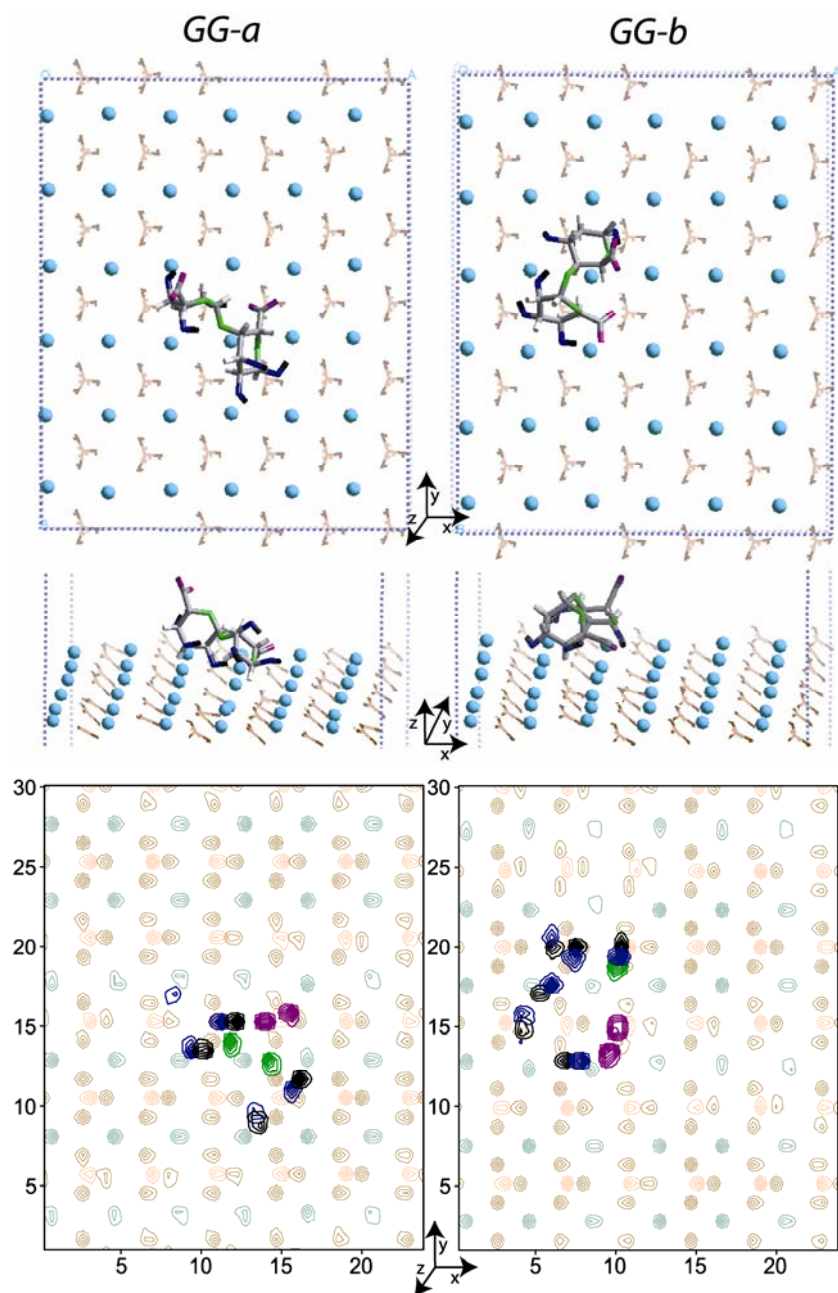


Figure 13. Results of molecular dynamics simulations (50 ps) of the GG alginic acid disaccharide started from the global potential energy minimum (a) conformation (left) and a local potential energy minimum (b) conformation (right) on the $(10\bar{1}4)$ calcite surface with explicit hydration. Water molecules have been removed for clarity. A representation of the disaccharides and calcite surface are apparent from a plan view in the upper frames and a side view in the middle frames. The bottom frames provide the atomic density contours of the disaccharide and calcite atoms derived from atomic trajectories for the course of the production simulation. All plot axes are distances (\AA) and represent the dimensions of the simulation cell. Atoms are color coded as follows for calcite: calcium (light blue), calcite carbon (light brown), and calcite oxygen (dark brown); for the disaccharide: carboxylate oxygen (purple), ether oxygen (green), hydroxyl oxygen (dark blue), and hydroxyl hydrogen (black).

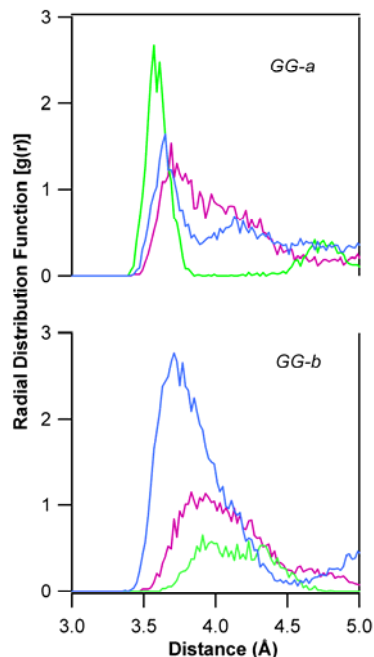


Figure 14. Radial distribution functions for Ca-O interactions for the disaccharide oxygen species and the calcium atoms in the first layer of calcite for the 50 ps simulation period. Hydroxyl (blue), carboxyl (red), and ether (green) oxygen species are colored similar to the representations in Figure 13.

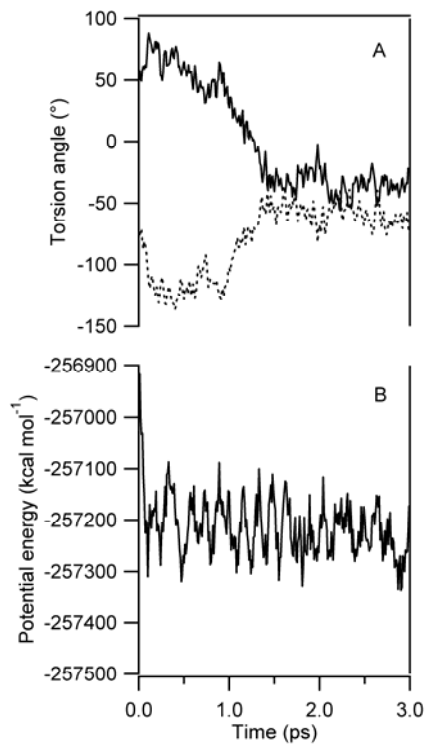


Figure 15. Variation in torsion angles (solid line, Φ ; dashed line, Ψ ; A) and potential energy (B) of the solvated *GG-b* disaccharide during the initial 3 ps of the equilibration run.

approximately 300 kcal mol⁻¹. Closer inspection of the torsion angles reveals that each variation in one of the torsion angles results in complementary opposing changes of the other, so as to reduce the steric hindrance of the remaining disaccharide structure and avoid destabilization.

While this study has expanded on the interactions of the *GG* disaccharide, similar analyses were conducted with *MM* and *MG* disaccharides (viz. Table 7 and Figure 12). A similar movement from the local energy conformation (*b*) to the global potential energy minimum (*a*) conformation is observed for all disaccharides when solvated (Table 7). The potential energy barrier for movement from the *b* to the *a* conformation is relatively low (<20 kcal mol⁻¹) and the transition has been shown to readily occur at 300 K for *GG* and *MM*.

MM-b is the only disaccharide to revert from the *b* conformation to the *a* conformation when associated with the calcite surface (Table 7). For other disaccharides, interaction with the calcite surface maintained the local energy minima conformation (Table 7) and the stabilization was the result of interactions of the disaccharide with surface cations (viz. Figures 13 and 14). The *MM-b* disaccharide has the lowest E_{sorp} with the calcite surface (viz. Figure 12) due to the β -linkage of the disaccharide and resultant equatorial orientation of the electron-donating and charged oxygens on the disaccharide. The strong Coulombic interactions of the carboxylate groups and their orientation due to the α linkages of the *GG* and *MG* disaccharides control their torsional rotation when associated with the calcite surface. Conversely, the more planar nature of the β -linkage on the *MM* disaccharide allows a less energetically-constrained rotation and fewer close-range repulsions with the calcite surface.

The presence of disaccharides disrupts hydration of the calcite surface (Figure 16). When the disaccharide is solvated in the bulk solution (viz. Figure 2), water molecules are coordinately arranged on the calcite surface. Water molecules can be associated with a single surface cation or can interact with two cations, and additionally be stabilized by forming hydrogen bonds with the surface carbonate species. A hydrogen bonding network also exists laterally among the first surface monolayer of waters and with the waters above. The doubly-associated surface water molecules are aligned with the y-axis of our simulation cells because the carbonate species on the (10 $\bar{1}$ 4) calcite surface project out of the cleavage plane (viz. Figure 13). The degree of coordination dramatically affects the residence times of the water molecules on the calcite surface (Perry et al., 2006). Previous reports have found that hydration of the surface occurs similarly to our results of single coordination (de Leeuw and Parker, 1997). However, the previous studies have modeled only a single monolayer of water on the calcite surface. As noted above, surface hydration will be further stabilized by additional layers of water and the formation of a hydrogen bonded network.

Disaccharides associated with the calcite surface affect calcite hydration (Figure 16). Association of the disaccharides causes displacement of water molecules from the surface and a reduction in the hydration. Additionally, it appears that the presence of the sorbed disaccharides induces ordering of the water molecules on the calcite surface. The observed increase in the double-coordination of water to calcium when the disaccharide is surface-associated may be the result of the absence of disruptive long-range forces in comparison to when the disaccharide is solvated in the bulk solution. The conformation of the disaccharide affects the shape and region of disrupted hydration. If the proper geometry is present, a disaccharide on the surface also

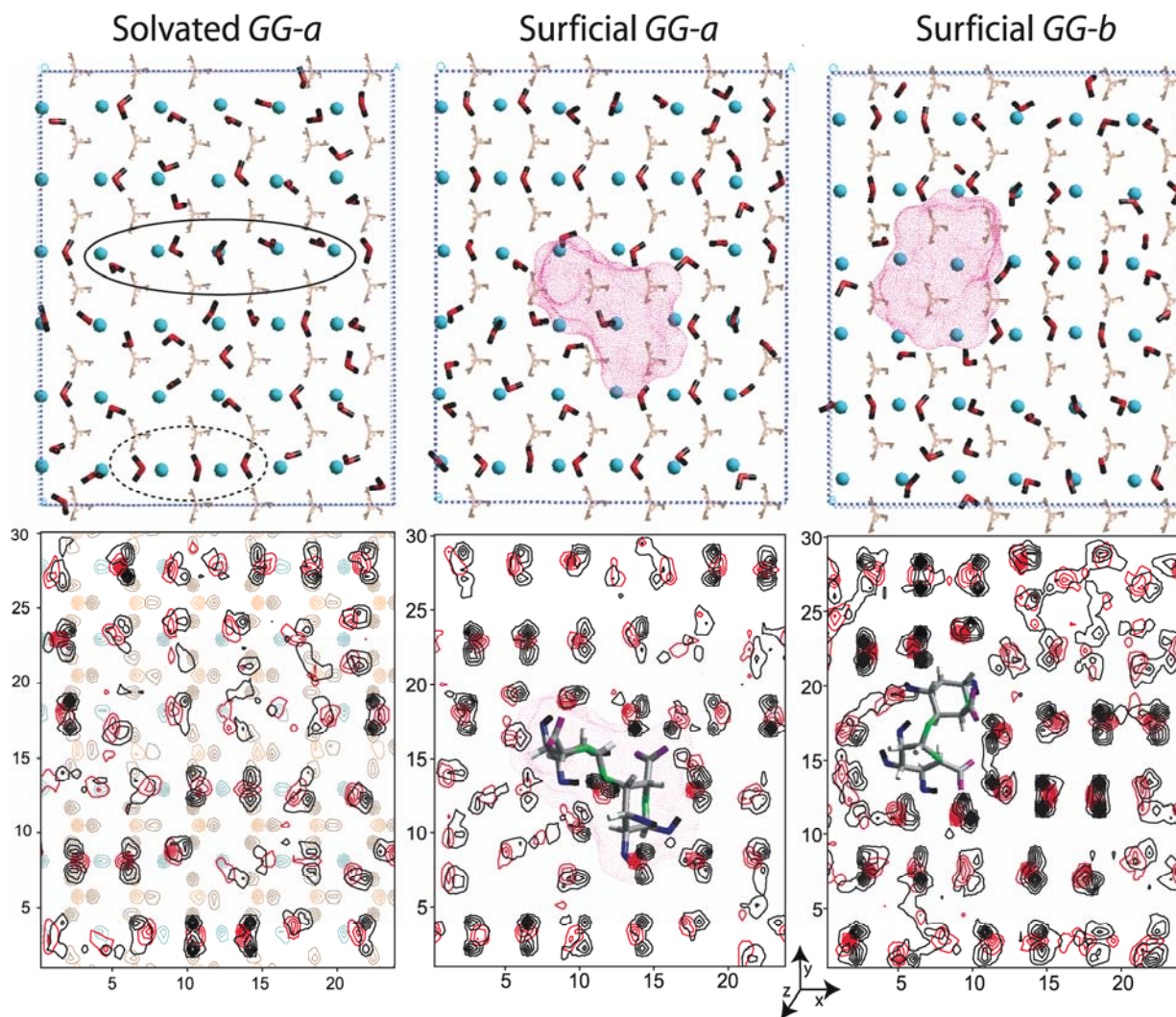


Figure 16. Molecular dynamics simulation (50 ps) of the GG alginic acid disaccharide solvated (left), and in the global (*a*; middle) and local (*b*; right) potential energy minimum conformations associated with the $(10\bar{1}4)$ calcite surface with explicit hydration. The top frames show the positions and conformations of the atoms near the calcite surface at 50 ps of the simulation. The bottom frames show the atomic density of the water and calcite atoms over the course of the simulation. Representations of the disaccharides with calculated Connolly surfaces and are superimposed to show the positions of the disaccharides. Water molecules interacting with single (solid line oval) and double (dashed line oval) surface cations are highlighted. All plot axes are distances (Å) and represent the dimensions of the simulation cell.

appears to be able to further stabilize hydration. The water molecule associated with the ether linkage of the *GG-a* disaccharide is associated with both the calcite calcium below and by hydrogen bonding to the disaccharide above. These coordinations result in an ordered and stabilized disaccharide with both water and surface species, as demonstrated by the dense array of contour lines for the atomic densities in Figure 13.

3.6. Alginic Acid Binding at a Surface Defect on the Calcite Surface

Calcite dissolution by a microbially-produced polysaccharide has been observed to occur via a crystallographically specific mechanism (Perry et al., 2004). Alginic acid has been observed to preferentially attack the obtuse steps of dissolution pits on the $(10\bar{1}4)$ calcite surface. We have begun to model the interactions of disaccharides at dissolution pits to understand their preferential attachment on the obtuse pit step. Previous work by us has hypothesized that imposed steric hindrance by the acute step limits the ability of alginic acid binding groups to form surface-active complexes and thereby limits ligand-promoted dissolution (Perry et al., 2004).

The energy landscape of a *GG-a* disaccharide about a dissolution pit was explored (Figure 17). The dissolution pit was created by manual removal of a monolayer of surface atoms from the $(10\bar{1}4)$ calcite surface. Molecular dynamics simulations were not conducted due to energy instabilities associated with the pit edges, most likely due to pit-pit interactions across cell boundaries in the periodic systems. Fortunately, the force field can accommodate static energy calculations for organics with these highly defective surface topologies. The *GG-a* disaccharide was systematically moved around the different vertices of the pit and energy minimization allowed an exploration of the disaccharide preference for different regions of the pit.

The *GG-a* disaccharide preferred coordination with the *oo* and *aa* vertices of the carbonate pit, as opposed to the *oa* and *ao* (Figure 17). Assuming that the relative impact of the surface of the pit bottom on disaccharide potential energy is the same at all four vertices, the destabilizing effect at any vertex must be the result of interactions with the pit edge. The *oo* and *aa* pit vertices terminate with a carbonate leaving two calcium ions relatively exposed. Conversely, the *oa* and *ao* vertices terminate with a calcium ion exposing two carbonates. The interactions of the disaccharide carboxylates with the calcite carbonates at these vertices likely control the observed instabilities. The disaccharide was more stable by 6 kcal mol⁻¹ at the *oo* vs. the *aa* vertex. An extended study of the association of the major disaccharides conformations with calcite pits and pit edges would necessarily be conducted with larger simulation cells and long-duration molecular dynamics simulations.

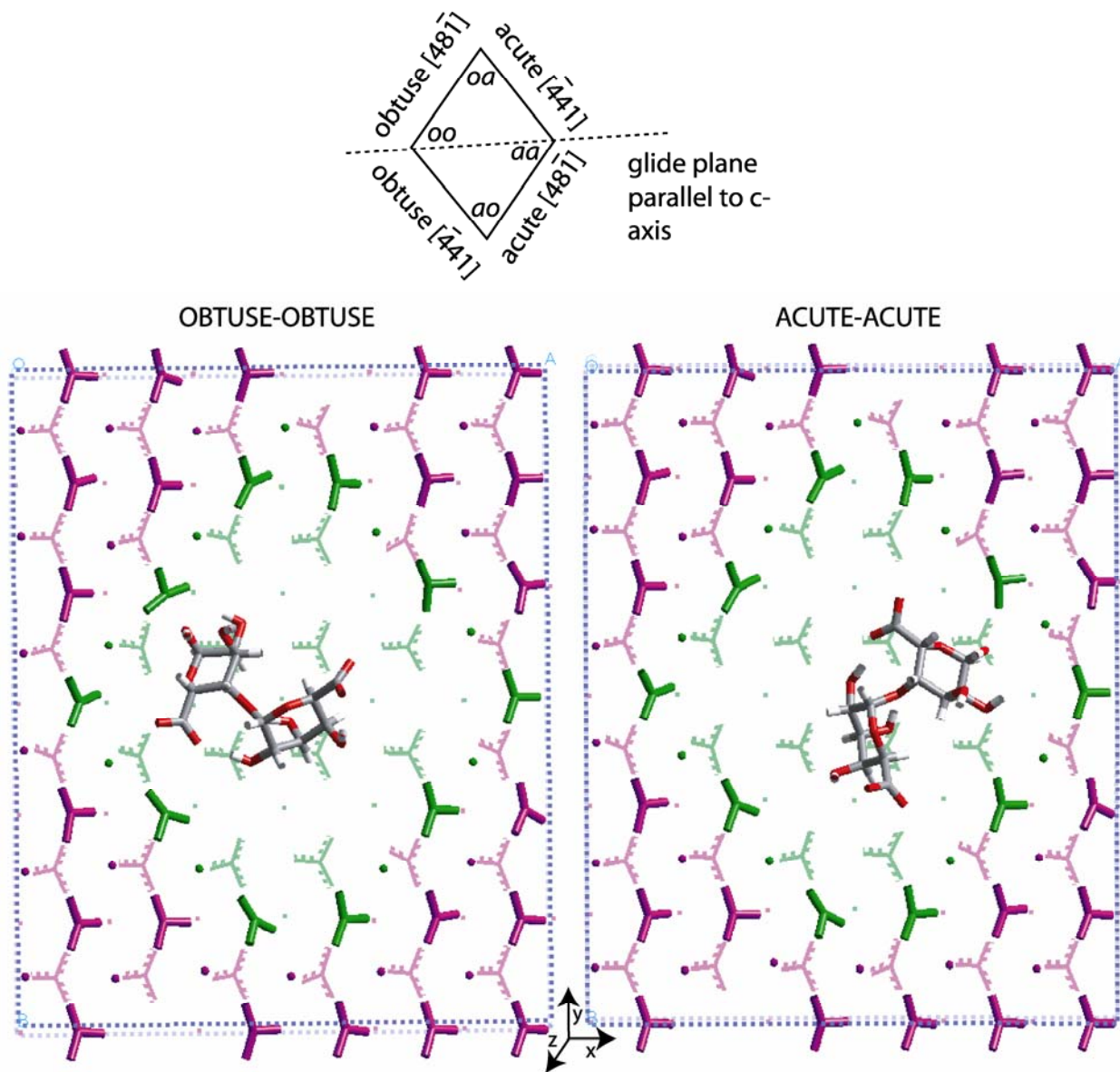


Figure 17. Top-down view of the energy-minimized conformations of GG-a disaccharides associated with the oo and aa edges of a dissolution pit in the $(10\bar{1}4)$ calcite surface. Top calcite plane is represented by cylindrical bonds while the second calcite plane is denoted by stick bonds. The pit is highlighted by green coloration. Disaccharide color key: red = oxygen, gray = carbon, white = hydrogen.

4. Conclusions

Atomistic-scale predictive modeling is well suited for the evaluation of organic-inorganic binding reactions, especially those associated with the polysaccharide-based exudates nominally represented by alginic acid. In this study, the effects of ether-linkage torsion, intramolecular interactions, cation binding, and temperature on the conformation and relative stabilities of different representative disaccharide and polysaccharides were evaluated. Based on the molecular dynamics simulation results represented in Figures 3-7, the expected variation in the torsion linkages of alginic acid disaccharides was evaluated (Table 5). We determine that, independent of starting conformation, the preferred conformation of disaccharides is primarily associated with the global potential energy minimum *a*. This assertion is extended to most *in situ* environments, including marine and terrestrial locations, due to the effect of deprotonation and temperature on driving the disaccharides to this minimum conformation. Most alginic acid *in situ* are expected to be deprotonated at the carboxylate functionalities due to their relatively low pK_a values. Torsional modification and molecular dynamics simulations indicate that deprotonated carboxylic groups on *MM*, *GG*, and *MG* disaccharides lead to an energetically favored conformation for all disaccharides at $\Phi = 274.1 \pm 7.2^\circ$, $\Psi = 227.2 \pm 4.8^\circ$. Intramolecular interactions within polymer chains stabilized some of the less-favored conformations. However, simulations of cation association with the disaccharides and polymers resulted in Coulombic interactions that greatly stabilized conformations removed from the global energy minimum. Calcium binding energies with the *MG* disaccharide and polymer indicate that these alternating monosaccharide blocks may have an underestimated role in cation binding in comparison to *MM* and *GG* alginate blocks (Emmerichs et al., 2004; Lattner et al., 2003). A hybrid energy force field for modeling interactions of organic molecules with carbonate mineral surface in hydrated environments was developed. This force field was used to investigate the interaction of alginic acid with the (10 $\bar{1}$ 4) calcite surface. Alginic acid disaccharides have a preferred conformation when solvated but have the ability to maintain other forms when associated with the calcite surface. The *GG-a* disaccharide forms the most stable complexes with the calcite surface. The differences in the binding energies of the different disaccharides are controlled by the proximity of electron-donating oxygen moieties on the disaccharides to cations on the calcite surface. The binding of organics to the calcite surface affects the amount and ordering of surface hydration. The force field can also be applied to simulation of mineral surfaces with defects.

5. References

- Aizenberg J., Tkachenko A., Weiner S., Addadi L., and Hendler G. (2001) Calcitic microlenses as part of the photoreceptor system in brittlestars. *Nature* **412**(6849), 819-822.
- Allen M. P. and Tildesley D. J. (1987) *Computer Simulation of Liquids*. Oxford University Press.
- Atkins E. D. T., Nieduszy.Ia, and Parker K. D. (1973a) Structural components of alginic acid: 1. Crystalline-structure of poly-beta-D-mannuronic acid—Results of X-ray-diffraction and polarized infrared studies. *Biopolymers* **12**(8), 1865-1878.
- Atkins E. D. T., Nieduszy.I, Parker K. D., and Smolko E. E. (1973b) Structural components of alginic acid: 2. Crystalline-Structure of poly-alpha-L-guluronic acid—Results of X-ray-diffraction and polarized infrared studies. *Biopolymers* **12**(8), 1879-1887.
- Banfield J. F., Barker W. W., Welch S. A., and Taunton A. (1999) Biological impact on mineral dissolution: Application of the lichen model to understanding mineral weathering in the rhizosphere. *Proceedings of the National Academy of Sciences of the United States of America* **96**(7), 3404-3411.
- Belitz H. and Grosch W. (1987) *Food Chemistry*. Springer.
- Berman A., Addadi L., and Weiner S. (1988) Interactions of sea-urchin skeleton macromolecules with growing calcite crystals—A study of intracrystalline proteins. *Nature* **331**(6156), 546-548.
- Boyd A. and Chakrabarty A. M. (1995) Pseudomonas Aeruginosa Biofilms - Role of the Alginate Exopolysaccharide. *Journal of Industrial Microbiology* **15**(3), 162-168.
- Braccini I., Grasso R. P., and Pérez S. (1999) Conformational and configurational features of acidic polysaccharides and their interactions with calcium ions: a molecular modeling investigation. *Carbohydrate Research* **317**(1-4), 119-130.
- Braccini I. and Pérez S. (2001) Molecular basis of Ca²⁺-induced gelation in alginates and pectins: the egg-box model revisited. *Biomacromolecules* **2**, 1089-1096.
- Christensen B. E. and Charaklis W. G. (1990) Physical and chemical properties in biofilms. In *Biofilms* (ed. W. G. Charaklis and K. C. Marshall). Wiley.
- Compton R. G. and Sanders G. (1993) The dissolution of calcite in aqueous acid: The influence of humic species. *Journal of Colloid and Interface Science* **158**, 439-445.
- Cygan R. T. (2001) Molecular modeling in mineralogy and geochemistry. In *Molecular Modeling Theory: Applications in the Geosciences*, Vol. 42 (ed. R. T. Cygan and J. D. Kubicki), pp. 1-35. Mineralogical Society of America.

- Dauber-Osguthorpe P., Roberts V. A., Osguthorpe D. J., Wolff J., Genest M., and Hagler A. T. (1988) Structure and energetics of ligand-binding to proteins: Escherichia-coli dihydrofolate reductase trimethoprim, a drug-receptor system. *Proteins: Structure, Function, and Genetics* **4**(1), 31-47.
- Davis T. A., Llanes F., Volesky B., and Mucci A. (2003) Metal selectivity of *Sargassum spp.* and their alginates in relation to their alpha-L-guluronic acid content and conformation. *Environmental Science and Technology* **37**(2), 261-267.
- de Leeuw N. H. and Cooper T. G. (2004) A computer modeling study of the inhibiting effect of organic adsorbates on calcite crystal growth. *Crystal Growth and Design* **4**(1), 123-133.
- de Leeuw N. H. and Parker S. C. (1997) Atomistic simulation of the effect of molecular adsorption of water on the surface structure and energies of calcite surfaces. *Journal of the Chemical Society Faraday Transactions* **93**(3), 467-475.
- de Yoreo J. J. and Dove P. M. (2004) Shaping crystals with biomolecules. *Science* **306**, 1301-1302.
- Dheu-Andries M. L. and Pérez S. (1983) Geometrical features of calcium-carbohydrate interactions. *Carbohydrate Research* **124**(2), 324-332.
- Didymus J. M., Oliver P., Mann S., DeVries A. L., Hauschka P. V., and Westbroek P. (1993) Influence of low-molecular-weight and macromolecular organic additives on the morphology of calcium carbonate. *Journal of the Chemical Society Faraday Transactions* **89**(15), 2891-2900.
- Duckworth O. W., Cygan R. T., and Martin S. T. (2003) Linear free energy relationships between dissolution rates and molecular modeling energies of rhombohedral carbonates. *Langmuir* **20**, 2938-2946.
- Effenberger H., Mereiter K., and Zemann J. (1981) Crystal structure refinements of magnesite, calcite, rhodochrosite, siderite, smithsonite, and dolomite, with discussion of some aspects of the stereochemistry of calcite type carbonates. *Zeitschrift für Kristallographie* **156**, 233-243.
- Emmerichs N., Wingender J., Flemming H.-C., and Mayer C. (2004) Interaction between alginates and manganese cations: identification of preferred cation binding sites. *International Journal of Biological Macromolecules* **34**, 73-79.
- Evans L. R. and Linker A. (1973) Production and characterization of the slime exopolysaccharide of *Pseudomonas aeruginosa*. *Journal of Bacteriology* **116**, 915-924.
- Fortey R. and Chatterton B. (2003) A Devonian trilobite with an eyeshade. *Science* **301**(5640), 1689.

- Fredd C. and Fogler H. (1998) The influence of chelating agents on the kinetics of calcite dissolution. *Journal of Colloid and Interface Science* **204**, 187-194.
- Grant G. T., Morris E. R., Rees D. A., Smith P. J. C., and Thom D. (1973) Biological interactions between polysaccharides and divalent cations—Egg-box model. *FEBS Letters* **32**(1), 195-198.
- Guenot J. and Kollman P. A. (1992) Molecular dynamics studies of a DNA-binding protein: 2. An evaluation of implicit and explicit solvent models for the molecular dynamics simulation of the *Escherichia coli* Trp repressor. *Protein Science* **1**(9), 1185-1205.
- Guimarães C. R. W., Barreiro G., de Oliveira C. A. F., and de Alencastro R. B. (2004) On the application of simple explicit water models to the simulations of biomolecules. *Brazilian Journal of Physics* **34**(1), 126-136.
- Halgren T. A. (1992) Representation of van der Waals (vdW) interactions in molecular mechanics force fields: Potential form, combination rules, and vdW parameters. *Journal of the American Chemical Society* **114**(20), 7827-7843.
- Hardalo C. and Edberg S. C. (1997) *Pseudomonas aeruginosa*: Assessment of risk from drinking water. *Critical Reviews in Microbiology* **23**(1), 47-75.
- Haug A., Myklesta S., Larsen B., and Smidsrød O. (1967) Correlation between chemical structure and physical properties of alginates. *Acta Chemica Scandinavica* **21**(3), 768-773.
- Henriksen K., Stipp S. L. S., Young J. R., and Bown P. R. (2003) Tailoring calcite: Nanoscale AFM of coccolith biocrystals. *American Mineralogist* **88**(11-12), 2040-2044.
- Hoch A. R., Reddy M. M., and Aiken G. R. (2000) Calcite crystal growth inhibition by humic substances with emphasis on hydrophobic acids from the Florida Everglades. *Geochimica et Cosmochimica Acta* **64**, 61-72.
- Hoog C., Rotondo A., Johnston B. D., and Pinto B. M. (2002) Synthesis and conformational analysis of a pentasaccharide corresponding to the cell-wall polysaccharide of the Group A *Streptococcus*. *Carbohydrate Research* **337**(21-23), 2023-2036.
- Hoover W. G. (1985) Canonical dynamics: Equilibrium phase-space distributions. *Physical Review A* **31**(3), 1695-1697.
- Iyer L. K. and Qasba P. K. (1999) Molecular dynamics simulation of α -lactalbumin and calcium binding c-type lysozyme. *Protein Engineering* **12**(2), 129-193.
- Jamialahmadi M. and Mullersteinhagen H. (1991) Reduction of calcium-sulfate scale formation during nucleate boiling by addition of EDTA. *Heat Transfer Engineering* **12**(4), 19-26.

- Kennedy A. F. D. and Sutherland I. W. (1987) Analysis of bacterial exopolysaccharides. *Biotechnology and Applied Biochemistry* **9**, 12-19.
- Kerisit S. and Parker S. C. (2004) Free energy of adsorption of water and calcium on the {10-14} calcite surface. *Chemical Communications*, 52-53.
- Kollman P. A. (1996) Advances and continuing challenges in achieving realistic and predictive simulations of the properties of organic and biological molecules. *Accounts of Chemical Research* **29**(10), 461-469.
- Lattner D., Flemming H.-C., and Mayer C. (2003) ¹³C-NMR study of the interaction of bacterial alginate with bivalent cations. *International Journal of Biological Macromolecules* **33**, 81-88.
- Martin J. P. (1971) Decomposition and binding action of polysaccharides in soil. *Soil Biology and Biochemistry* **3**, 33-41.
- Moore R. E., Brennema, Dr, Bischof A. E., and Robins J. D. (1972) One-step anhydrite scale removal. *Materials Protection and Performance* **11**(3), 41-48.
- Orme C., Noy A., Wierzbicki A., McBride M., Grantham M., Teng H., Dove P., and DeYoreo J. (2001) Formation of chiral morphologies through selective binding of amino acids to calcite surface steps. *Nature* **411**, 775-779.
- Perry T. D., Cygan R. T., and Mitchell R. (2006) Molecular mechanics force field for modeling carbonate mineral surfaces with explicit hydration. *Physical Chemistry Chemical Physics*, in press.
- Perry T. D., Duckworth O. W., Kendall T. A., Martin S. T., and Mitchell R. (2005) Chelating ligand alters the microscopic mechanism of mineral dissolution. *Journal of the American Chemical Society* **127**, 5744-5745.
- Perry T. D., Duckworth O. W., McNamara C. J., Martin S. T., and Mitchell R. (2004) Effects of the biologically produced polymer alginic acid on macroscopic and microscopic calcite dissolution rates. *Environmental Science and Technology* **38**, 3040-3046.
- Pilson M. (1998) *An Introduction to the Chemistry of the Sea*. Prentice Hall.
- Reeder R. J., Nugent M., Tait C., Morris D., Heald S., Beck K., Hess W., and Lazirotti A. (2001) Coprecipitation of uranium(VI) with calcite: XAFS, micro-XAS, and luminescence characterization. *Geochimica et Cosmochimica. Acta* **65**, 3491-3503.
- Sabra W., Zeng A.-P., and Deckwer W.-D. (2001) Bacterial alginate: physiology, product quality and process aspects. *Applied Microbiology and Biotechnology* **56**, 315-325.

- Saiz-Jimenez C. (1999) Biogeochemistry of weathering processes in monuments. *Geomicrobiology Journal* **16**, 27-37.
- Schlesinger W. H. (1997) *Biogeochemistry: An Analysis of Global Change*. Academic Press.
- Smidsrød O. and Haug A. (1965) Effect of divalent metals on properties of alginate solutions: I. Calcium Ions. *Acta Chemica Scandinavica* **19**(2), 329-335.
- Söllner C., Burghammer M., Bush-Nentwich E., Berger J., Schwarz H., Riekel C., and Nicolson T. (2003) Control of crystal size and lattice formation by starmaker in otolith biomineralization. *Science* **302**, 282-286.
- Stahl G., Patzay G., Weiser L., and Kalman E. (2000) Study of calcite scaling and corrosion processes in geothermal systems. *Geothermics* **29**, 105-119.
- Stumm W. (1992) *Chemistry of the Solid-Water Interface*. Wiley.
- Stumm W. and Morgan J. J. (1996) *Aquatic Chemistry*. Wiley.
- Suess E. (1970) Interaction of organic compounds with calcium carbonate-I. Associated phenomena and geochemical implications. *Geochimica et Cosmochimica Acta* **34**, 157-168.
- Sun H., Ren P., and Fried J. R. (1998) The COMPASS force field: Parameterization and validation for phosphazenes. *Computational and Theoretical Polymer Science* **8**(1-2), 229-246.
- Teng H. H., Dove P. M., Orme C. A., and De Yoreo J. J. (1998) Thermodynamics of calcite growth: baseline for understanding biomineral formation. *Science* **282**, 724-727.
- Thomas M., Clouse J., and Longo J. (1993) Adsorption of organic compounds on carbonate minerals 3. Influence on dissolution rates. *Chemical Geology* **109**, 227-237.
- Tosi M. P. (1964) Cohesion of ionic solids in the Born model. *Solid State Physics* **131**, 533-545.
- Verlet L. (1967) Computer 'experiments' on classical fluids: I. Thermodynamical properties of Lennard-Jones molecules. *Physical Review A* **195**, 98-103.
- Welch S. A., Barker W. W., and Banfield J. F. (1999) Microbial extracellular polysaccharides and plagioclase dissolution. *Geochimica et Cosmochimica Acta* **63**(9), 1405-1419.
- Welch S. A. and Vandevivere P. (1994) Effect of microbial and other naturally occurring polymers on mineral dissolution. *Geomicrobiology Journal* **12**, 227-238.
- Whitting S. (1971) Conformational energy calculations on alginic acid .1. Helix parameters and flexibility of homopolymers. *Biopolymers* **10**(9), 1481-1489.

Wolfgang M. C., Kulasekara B. R., Liang X. Y., Boyd D., Wu K., Yang Q., Miyada C. G., and Lory S. (2003) Conservation of genome content and virulence determinants among clinical and environmental isolates of *Pseudomonas aeruginosa*. *Proceedings of the National Academy of Sciences of the United States of America* **100**(14), 8484-8489.

Wu Y. and Grant C. (2002) Effect of chelation chemistry of sodium polyaspartate on the dissolution of calcite. *Langmuir* **18**, 6813-6820.

Distribution

- 1 Fawwaz Habbal
Division of Engineering and Applied Sciences
Harvard University
Pierce Hall 219
29 Oxford Street
Cambridge, MA 02138
- 1 Scot T. Martin
Division of Engineering and Applied Sciences
Harvard University
Pierce Hall 122
29 Oxford Street
Cambridge, MA 02138
- 5 Ralph Mitchell
Division of Engineering and Applied Sciences
Harvard University
Pierce Hall 127
29 Oxford Street
Cambridge, MA 02138
- 1 Venkatesh Narayanamurti
Division of Engineering and Applied Sciences
Harvard University
Pierce Hall 217A
29 Oxford Street
Cambridge, MA 02138
- 5 Todd D. Perry
Division of Engineering and Applied Sciences
Harvard University
Engineering Sciences Lab 304
40 Oxford Street
Cambridge, MA 02138
- 1 MS 0123 D. L. Chavez, 1011
1 MS 0123 M. L. Garcia, 1010
1 MS 0123 H. R. Westrich, 1011
1 MS 0310 S. L. Rempe, 8333
1 MS 0734 T. M. Nenoff, 6245
1 MS 0735 S. J. Altman, 6115
1 MS 0754 L. J. Criscenti, 6118
10 MS 0754 R. T. Cygan, 6118
1 MS 0754 J. A. Greathouse, 6118

1	MS 0754	T. E. Hinkebein, 6118
1	MS 0754	M. D. Nyman, 6118
1	MS 0754	N. Ockwig, 6118
1	MS 0889	J. W. Braithwaite, 1825
1	MS 0895	A. Martino, 8332
1	MS 1231	A. D. Romig, 0004
1	MS 1349	C. J. Brinker, 1002
1	MS 1411	M. S. Kent, 8332
1	MS 1411	M. J. Stevens, 8332
1	MS 1411	J. A. Voigt, 1846
1	MS 1413	B. C. Bunker, 1141
1	MS 1413	L. J. Frink, 8333
1	MS 1413	G. S. Heffelfinger, 8330
1	MS 1415	J. C. Barbour, 1110
1	MS 1415	P. J. Feibelman, 1114
1	MS 1415	K. Leung, 1114
1	MS 9054	T. A. Michalske, 8300
2	MS 9018	Central Technical Files, 8945-1
2	MS 0899	Technical Library, 4536



Sandia National Laboratories